EVERLASTING

Electric Vehicle Enhanced Range, Lifetime And Safety Through INGenious battery management

D1.3 – Report on virtual test benches (MiL, SiL, HiL)

August 2019

This project has received funding from the European Union's Horizon 2020 research and innovation programme under grant agreement No 713771

Public

PROJECT SHEET	
Project Acronym	**EVERLASTING**
Project Full Title	Electric Vehicle Enhanced Range, Lifetime And Safety Through INGenious battery management
Grant Agreement	**713771**
Call Identifier	H2020-GV8-2015
Topic	GV-8-2015: Electric vehicles' enhanced performance and integration into the transport system and the grid
Type of Action	Research and Innovation action
Project Duration	48 months (01/09/2016 – 31/08/2020)
Coordinator	VLAAMSE INSTELLING VOOR TECHNOLOGISCH ONDERZOEK NV (BE) - *VITO*
Consortium Partners	COMMISSARIAT A L ENERGIE ATOMIQUE ET AUX ENERGIES ALTERNATIVES (FR) - *CEA* SIEMENS INDUSTRY SOFTWARE SAS (FR) - *Siemens PLM* TECHNISCHE UNIVERSITAET MUENCHEN (DE) - *TUM* TUV SUD BATTERY TESTING GMBH (DE) - *TUV SUD* ALGOLION LTD (IL) - *ALGOLION LTD* RHEINISCH-WESTFAELISCHE TECHNISCHE HOCHSCHULE AACHEN (DE) - *RWTH AACHEN* LION SMART GMBH (DE) - *LION SMART* TECHNISCHE UNIVERSITEIT EINDHOVEN (NL) - *TU/E* VOLTIA AS (SK) - *VOLTIA* VDL ENABLING TRANSPORT SOLUTIONS (NL) – *VDL ETS*
Website	www.everlasting-project.eu

DELIVERABLE SHEET	
Title	**D1.3 – Report on virtual test benches (MiL, SiL, HiL)**
Related WP	WP1 (WP1 Task T1.3: Virtual test benches)
Lead Beneficiary	SIEMENS PLM
Author(s)	Matthieu Ponchant (SIEMENS PLM)
Reviewer(s)	Mario Paroha (Voltia) Camiel Beckers (TU/e)
Type	Report
Dissemination level	PUBLIC
Due Date	August 31, 2019 (M36)
Submission date	September 30, 2019 (M37)
Status and Version	Final, version 1.0

REVISION HISTORY			
Version	**Date**	**Author/Reviewer**	**Notes**
V0.1	06/08/2019	Matthieu Ponchant (SIEMENS PLM) Lead Beneficiary	First draft
V0.2	12/09/2019	Matthieu Ponchant (SIEMENS PLM) Lead Beneficiary	Draft finalization
V0.2	13/09/2019	An Li (SIEMENS PLM)	Peer review
V0.3	23/09/2019	Camiel Beckers (TU/e)	Quality check
V0.4	25/09/2019	Mario Paroha	Quality check
V1.0	30/09/2019	Carlo Mol (VITO) Coordinator	Submission to the EC

DISCLAIMER

The opinion stated in this report reflects the opinion of the authors and not the opinion of the European Commission.

All EVERLASTING consortium members are committed to publish accurate information and take the greatest care to do so. However, the EVERLASTING consortium members cannot accept liability for any inaccuracies or omissions nor do they accept liability for any direct, indirect, special, consequential or other losses or damages of any kind arising out of the use of this information.

ACKNOWLEDGEMENT

This project has received funding from the European Union's Horizon 2020 research and innovation programme under grant agreement No 713771

EXECUTIVE SUMMARY

The report summarizes the work done for the development of different virtual test bench models. The objectives of such model are the capability to model the complete vehicle for different scopes, like energy management purpose or battery management system (BMS) control calibration / validation.

A focus on the BMS development process is done in this document, especially through the description of the three different approaches from Model in the Loop (MiL) to Hardware in the Loop (HiL) with intermediate step the Software in the Loop (SiL). Each approach is relevant to reach a complete validation of BMS control strategies. At first, a plant model (physical model) has been developed, with basic control function, and validated. Then, a real BMS function has been developed and calibrated. Finally, the BMS control has been tested on real time platform (dSPACE RTI1016 platform) to ensure BMS consistency all the time through different scenarios, like fast charging or driving cycles.

TABLE OF CONTENTS

List of Abbreviations and Acronyms

ACRONYM	DEFINITION
BMS	Battery Management System
DC	Direct Current
DOW	Description of Work
HiL	Hardware in the Loop
HV	High Voltage
HVAC	Heat Venting Air Conditioning
I/O	Input / Output
LV	Low Voltage
MiL	Model in the Loop
NEDC	New European Driving Cycle
OCV	Open Circuit Voltage
PID	Proportional Integral (Derivate)
SiL	Software in the Loop
SOC	State of Charge
OCV	Open Circuit Voltage
VCU	Vehicle Control Unit
WLTP	World Harmonised Light Vehicle Test Procedure
WP	Work Package
WPL	Work Package Leader

LIST OF FIGURES

LIST OF TABLES

INTRODUCTION

Work package 1 aims at developing new models and tools supporting advanced BMS research and the individual development work packages through the research and development of new battery pack validation tools, supporting BMS design and calibration. This will be achieved through the research, development and delivery of virtual test benches enabling BMS coupling for testing (from MiL to HiL) and preliminary calibration in WP's 2...5.

BMS design and calibration processes require a multi-physical approach, because signal used in BMS are not only electrical but also thermal, like temperature. Indeed, in this project ageing and thermal runaway managements are key element to enhance the battery lifetime and increase the range of the vehicle.

Realistic performance scenarios like the WLTP or NEDC driving cycle [1] are also important to consider, especially the interaction between the battery and the electric powertrain and the vehicle environment. Indeed, electric vehicle must satisfy regulation in term of safety and range prediction must be performed by electric vehicle for helping final customer.

Such complex physical interactions can be easily handled with multi-physical modelling software, like Simcenter Amesim (Figure 1) [2]. Then not only plant modelling has to be considered, but also the control modelling and their connexion to correctly evaluate the BMS function and finally, with real hardware developed by LION SMART.

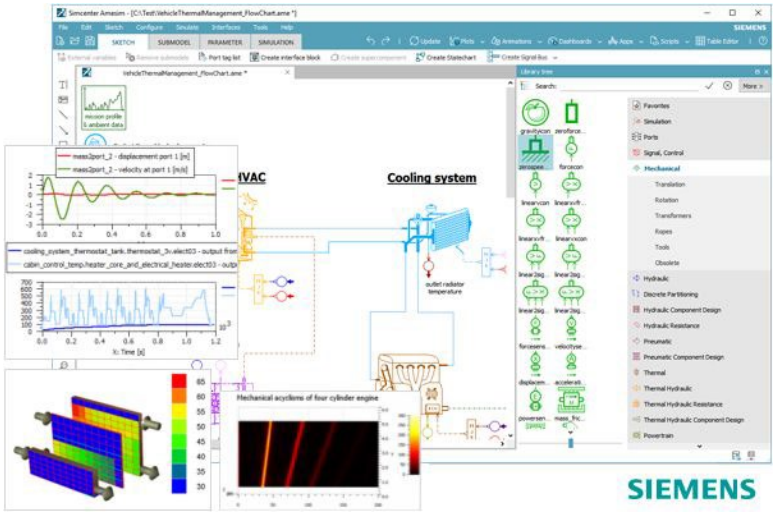

Figure 1: Modelling and simulation with Simcenter Amesim

At first, a model will be described with all subsystems in a MiL context. There are two levels of battery pack model; one dedicated to thermal management and the second one dedicated to BMS. A focus on co-simulation and real-time capability will be highlighted to ensure consistency between several levels of testing, especially for the virtual test bench with detailed battery pack model, which is described later.
Then, an example of coupling strategy and example will be highlighted for BMS function calibration and /or validation in SiL context. A focus on coupling with MATLAB/Simulink will be done to validate interface and communication between the two simulation platforms. Finally, a HiL virtual test bench will be described and an example will be provided on dedicated machine and functional BMS.

As this is a public document, confidential parameters have been replaced by default ones to highlight the virtual test bench methodology. Nevertheless, the results are still relevant and represent a realistic scenario.

1 MiL VIRTUAL TEST BENCHES

In the development process, Model in the Loop is the first step, allowing for a detailed physical (plant) model with functional control. The objectives of such model are:

- Validation of the plant model
- Preparation of the connexion with control without co-simulation constraints
- Faster simulation for subsystem assessment/trade-off.

In this project, the main goal is the development of tools supporting the BMS design and calibration. Thus plant model is limited to main subsystems like powertrain, electric network and thermal management system for one of both virtual test benches. The HVAC (Heat Venting Air Conditioning) is not considered in this virtual test bench but could be integrated with regards to the WP5 works linked to the active and passive cooling of the battery pack.

1.1 SUBSYSTEM DESCRIPTION

In a complete system level (vehicle), all subsystem must be studied and analysed as standalone. Nevertheless, in this project vehicle is already available and thus vehicle model has been directly realised. The vehicle under evaluation is electric utility van (eVan) supplied by Voltia. The eVan is a Citroen Jumper converted to a pure electric drive with swappable traction battery, as shown in Figure 2.

Figure 2: Electric utility van (eVan) from Voltia

Four main subsystems are described below:

- the powertrain, i.e. everything related to mechanical parts of the vehicle
- the electric network from battery pack to eMotors and electrical auxiliaries
- the functional BMS control, which will be partially replaced in SiL and HiL environment
- cooling system (only used in range estimator model)

1.1.1 POWERTRAIN MODEL

The powertrain is composed of all mechanical parts from the electric motor to the vehicle, as illustrated in Figure 3. A functional driver model has been added to follow driving cycle like the WLTP. Ambient conditions are considered as well, especially when thermal management is handled.

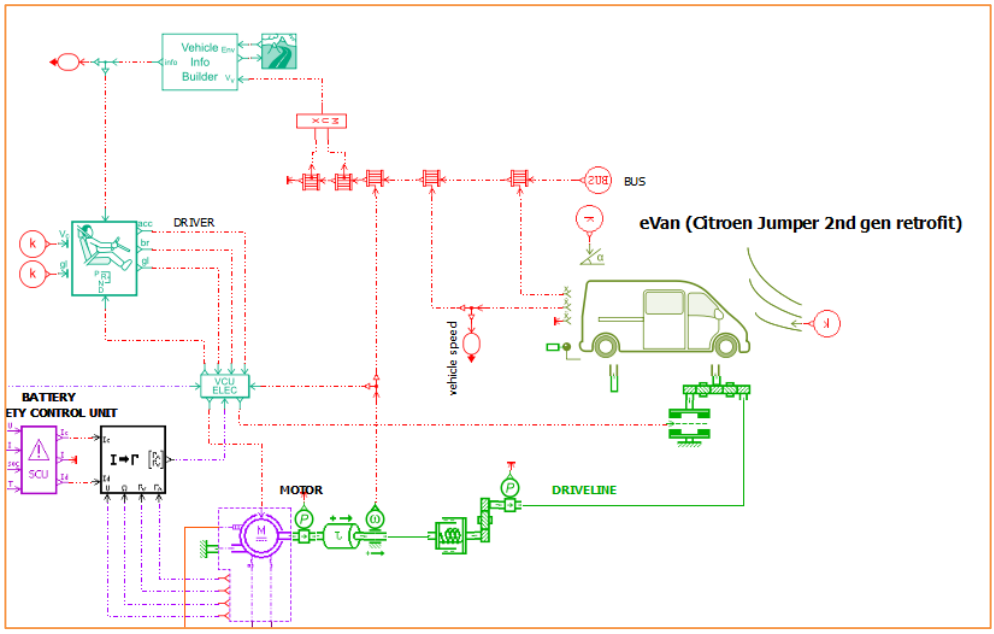

Figure 3: Powertrain subsystem

The driver subsystem is basically composed of 3 components:

- The driving cycle definition
- An equivalent PID controller for acceleration
- An equivalent PID controller for braking

Control of acceleration and braking is based on the vehicle error ϵ_{speed}(between vehicle speed in m/s and control speed in m/s) expressed as follow:

$$Command = k_{prop} \cdot \epsilon_{speed} + k_{int} \cdot \int \epsilon_{speed} + k_{antic} \cdot d\epsilon_{speed}$$

With ϵ_{speed} the speed error in m/s, k_{prop} the proportional gain in $(m/s)^{-1}$, k_{int} the integral gain in 1/m and k_{antic} the anticipative gain in $(m/s^2)^{-1}$.

Parameters of this components are detailed in Table 1.

Table 1: Driver component parameters

Driver parameters	Value	Units
Driving cycle	WLTP, NEDC…	m/s
Acceleration proportional gain	1	1/(m/s)
Acceleration integral gain	0.1	1/(m)
Acceleration anticipative (derivate) gain	0.1	1/(m/s^2)
Braking proportional gain	0.5	1/(m/s)
Braking integral gain	0.05	1/(m)
Braking anticipative (derivate) gain	0.05	1/(m/s^2)

The driving cycle is defined as a file where vehicle speed in m/s is a function of time in s, as illustrated with WLTP in Figure 4.

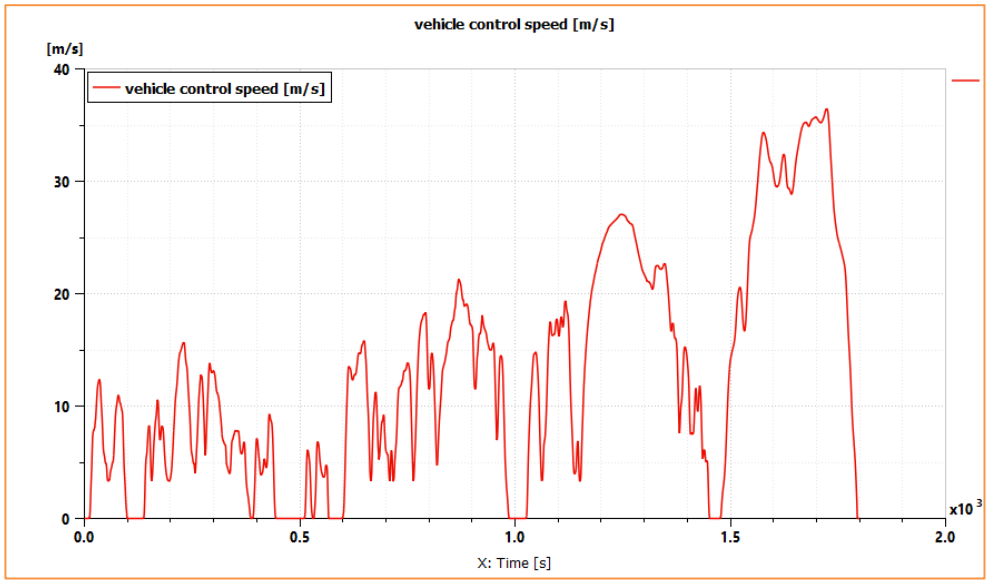

Figure 4: WLTP driving cycle

The vehicle component is used to compute resistive load of vehicle combining rolling resistance, drag and eventually climbing force in N, then the acceleration a in m/s^2, vehicle speed v in m/s and displacement x in m of the vehicle as follow:

$$a = \frac{F_{drag} + F_{roll} + F_{climb}}{M_{vehicle} + \frac{I_{wheel}}{R_{wheel}^2}}$$

$$F_{drag} = 0.5 \cdot \rho \cdot S \cdot Cx \cdot v^2$$

$$F_{roll} = R_{roll} \cdot M \cdot g \cdot \cos\left(\alpha \cdot \frac{\pi}{180}\right)$$

$$F_{climb} = M \cdot g \cdot \sin\left(\alpha \cdot \frac{\pi}{180}\right)$$

$$v = \int a \cdot dt$$

$$x = \int v \cdot dt$$

With ρ the air density in kg/m^2, S the frontal area in m^2, Cx the drag coefficient, g the gravity in m/s^2 and α the slope of the road in degree.

Parameters of these components are detailed in Table 2.

Table 2: Vehicle component parameters

Vehicle parameters	Symbol	Value	Units
Vehicle mass	M	2500	kg
Rolling resistance	F_{roll}	0.001	-
Drag coefficient	Cx	0.4	-
Frontal area	S	5	m^2
Wheel radius	R_{wheel}	0.35	m
Wheel inertia	I_{wheel}	0.1	kg.m^2

The braking command from the driver is transferred to a brake model applying a braking torque in Nm to the vehicle wheel. Maximum torque has been set at 2000 Nm, corresponding to the sum of regenerative and hydraulic braking.

The wheel is not directly connected to the motor shaft to limit size of the motor. So, a transmission with fixed gear ratio has been integrated between both. Its gear ratio is around 8 to allow higher motor speed and limited motor torque. As in any machinal component, losses in this gearbox must be considered. In this study, these losses have been integrated in the motor losses, as explained later in the electric network.

The drivetrain is composed of a shaft model with its own damping and stiffness to compute motor speed based on its torque and wheel torque. An equivalent shaft inertia J_{equi} in kg.m^2 can be considered to limit the complexity of the system. Indeed, motor shaft inertia $J_{motor\ shaft}$ in kg.m^2 can be combined with wheel shaft inertia $J_{wheel\ shaft}$ in kg.m^2 by considering the gear ratio i_g as follow:

$$J_{equi} = J_{motor\ shaft} + i_g^2 \cdot J_{wheel\ shaft}$$

Parameters of these components are detailed in Table 3.

Table 3: Drivetrain component parameters

Vehicle parameters	Value	Units
Shaft inertia	0.5	Kg.m^2
stiffness	100	Nm/degree
Damping coefficient	10	Nm/(rev/min)

The electric motor (e-motor) component is a mapped based model and takes also the inverter losses into account in this study. Motor is defined by its maximal propulsion and regenerative torque in Nm as a function of the motor speed in rev/min.

The overall drivetrain losses have been experimentally estimated by the University of Eindhoven in this project [3]. These losses are function of the motor speed in rev/min and torques (propulsion or regenerative) in Nm as illustrated in Figure 5 are a combination of the following losses:

- Inverter losses
- Motor losses
- Gear ratio losses
- Wheel hub losses

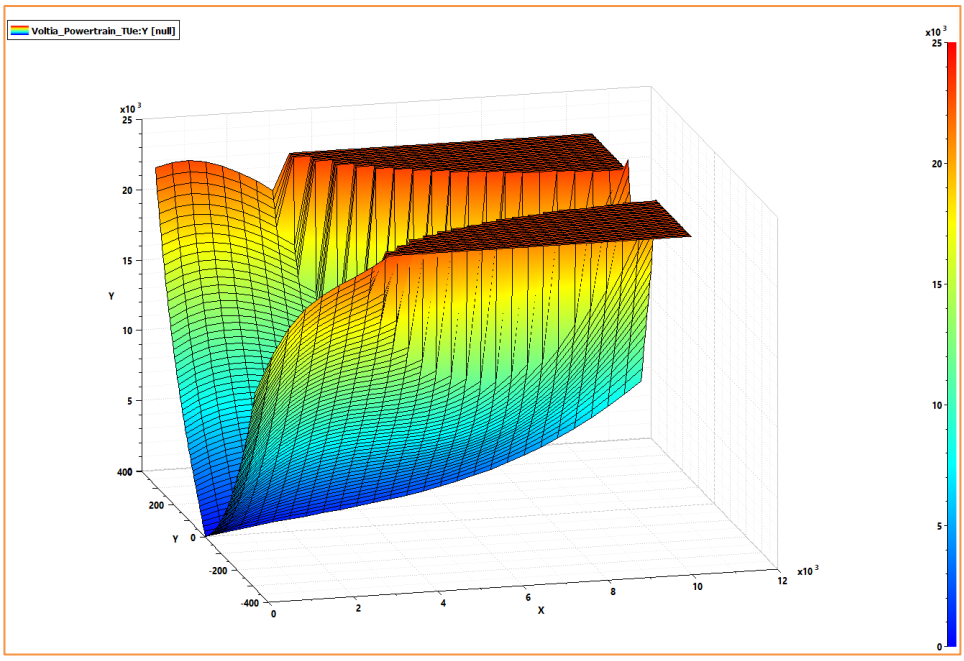

Figure 5: eVan overall driveline losses as function of torque and motor speed

With torque T_{motor}, speed $\omega_{motor}$and losses, efficiency ϵ is calculated and motor current I_{equi} in A is then computed as follows:

$$I_{motor} = \frac{T_{motor} \cdot \omega_{motor}}{\epsilon \cdot U_{motor}} \; if \; T_{motor} > 0$$
$$= \epsilon \cdot \frac{T_{motor} \cdot \omega_{motor}}{U_{motor}} \; if \; T_{motor} < 0$$

With ϵ the motor efficiency and U_{motor} the voltage at inverter input.

1.1.2 ELECTRIC NETWORK MODEL

The electric circuit is composed of all electrical parts in the vehicle from the voltage source (battery) to all current consumers, as illustrated in Figure 6. Basically, the electric circuit is composed of the high voltage (HV) and low voltage (LV) circuits, connected together through a DC/DC converter.

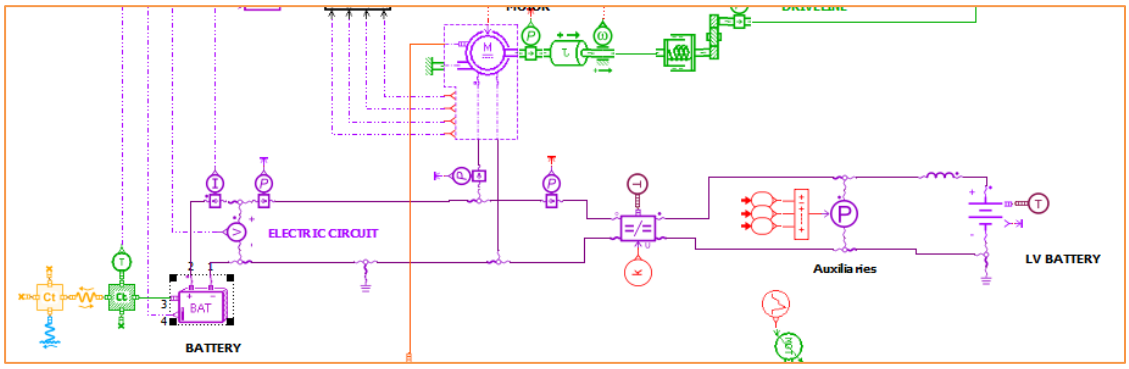

Figure 6: Electric circuit subsystem

The e-motor described in the previous section (1.1.1) is the main current consumer. In this simplified electric circuit, the LV circuit has been integrated to consider the LV consumers like electric pump, fan, blower which are negligible when vehicle is running but could have an impact when the vehicle is standing still, because battery SOC is affected. For example, during charging period, battery cooling could be activated to limit the temperature rise and avoid risk of thermal runaway. LV auxiliaries have been modelled with a power source. To simplify the model, all electrical power source (see 1.1.4 for details) have been grouped together.

A LV battery has been added and corresponds to the conventional Lead-Acid battery of the vehicle. The OCV in V is determined from the SOC in % as illustrated in Figure 7, which is calculated with current I in A received as follows:

$$SOC = 100 \cdot \int \frac{I}{C_{nom}} \cdot dt$$

With C_{nom} the nominal capcity in Ah.

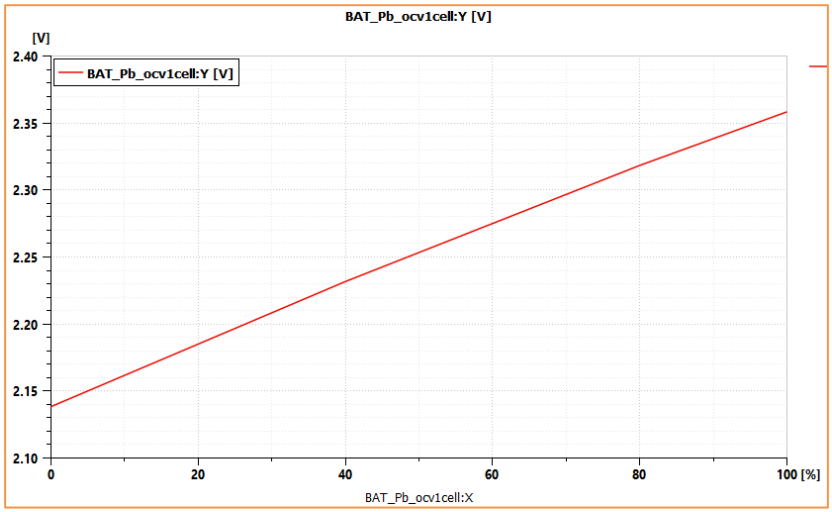

Figure 7: Lead-Acid OCV function of the SOC

Then the low voltage U_{bat} in V is calculated from OCV, current and internal resistance as follows:

$$\frac{dU_{bat}}{dt} = \frac{I - \frac{(U - OCV)}{R \cdot Ns}}{Cf}$$

With R the internal cell resistance in Ohm, Ns the number of cell in series and Cf the filtering capacitance in F (numerical parameters[1]).

Parameters of these components are detailed in Table 4.

Table 4: Lead acid battery component parameters

Vehicle parameters	Value	Units
Cells in series	6	-
Nominal capacity	70	Ah
Internal resistance per cell	0.00225	Ohm
Filtering capacitance	2	F

The LV circuit is connected to the HV circuit with a DC/DC converter. A functional model is used to compute HV current based on low (set at 13.9 V) and high voltage and current from LV circuit as follows:

$$I_{HV} = \eta \cdot I_{LV} \cdot \frac{U_{LV}}{U_{HV}}$$

With η the efficiency of the DC/DC converter set at 0.75.

This battery is assumed to work at constant temperature (ambient temperature) unlike the HV battery.

The last component of the electric circuit is the HV battery composed of 18650 nickel-rich, silicon-graphite lithium-ion cells of 3.35 Ah [4]. The detailed model of the cell is described in [4] and corresponds to an equivalent circuit model. In the context of virtual test bench, not only the cell is considered but the whole battery pack with electrical and thermal behaviour. Based on the aim of the model, the battery pack can be refined or not. In this section, battery is considered as a single component composed of all the cells[2]. The battery cell material has been estimated thanks to test measurement done on the cell [5]. The battery pack casing is assumed to be made of aluminium.

The parameters of the battery pack are detailed in Table 5.

[1] The value will be explained in the section 1.3.133
[2] A second level of model which is more detailed is proposed in section 1.3.1

Table 5: Lithium-ion battery pack component parameters

Vehicle parameters	Value	Units
Cells in series	2000	-
Cell in parallel	15	-
Cell mass	0.04622	kg
Battery casing mass	10	kg
Thermal conductance between cells and casing	20	W/m^2/degC
Contact surface between cells and casing	3	m^2
Convective heat exchange coefficient	20	W/m^2/degC
Convective heat exchange surface	1	m^2

1.1.3 FUNCTIONAL CONTROL

All physical subsystems are composed of actuators, which must be controlled, as illustrated in Figure 8. In this study, three main functions have been modelled:

- Vehicle Control Unit (VCU)
- Battery safety control unit
- E-motor control

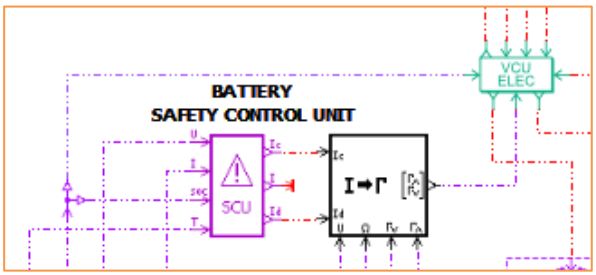

Figure 8: Functional control subsystem

The VCU receives as input acceleration & braking commands from the driver model. The E-motor torque request is then calculated as follows:

$$T_{req} = acc \cdot T_{max}$$

With acc the acceleration command and T_{max} the maximum torque available from the E-motor control in Nm.

Regenerative braking is available, and vehicle is slowed down by e-motor until maximum regenerative torque. Then conventional braking torque is applied to complete the required braking command as illustrated in Figure 9.

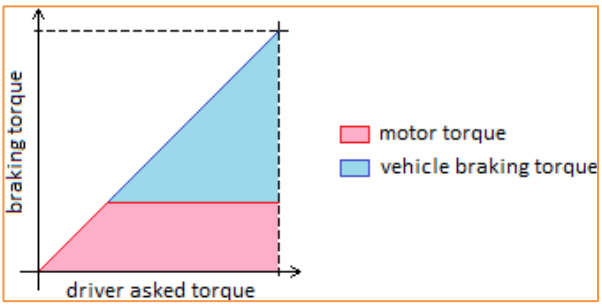

Figure 9: Regenerative braking strategy

The battery safety control is integrated to estimate the maximum admissible current, as illustrated in Figure 10 either for charging I_{max} or discharging I_{min} in A, expressed as follow:

$$I_{min} = \frac{U_{min} - U}{R_{eq}}$$
$$I_{max} = \frac{U_{max} - U}{R_{eq}}$$

With U_{min} the minimum battery voltage in V, U_{max} the maximum battery voltage in V and R_{eq} the equivalent battery resistance in Ohm.

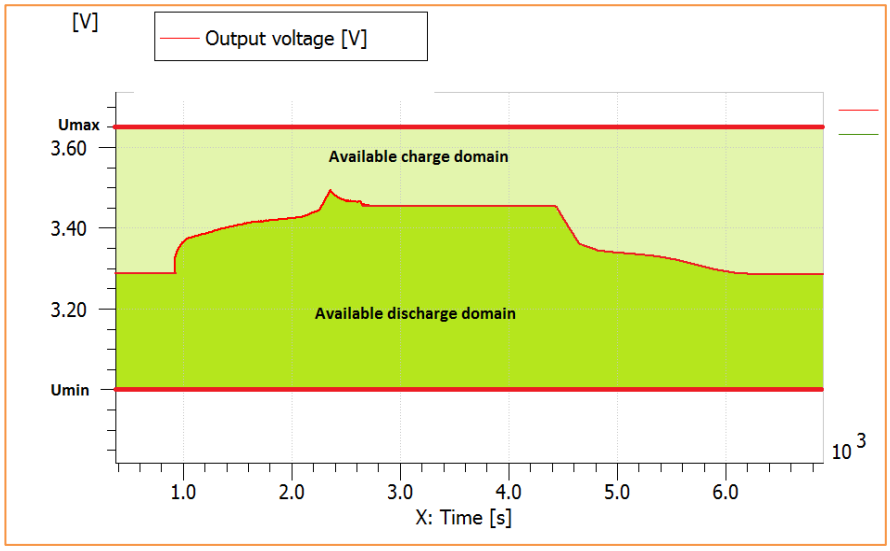

Figure 10: Battery safe voltage domain

The E-motor control is used to check if maximum torque in Nm for a dedicated motor speed is higher than maximum torque available from battery power as illustrated in Figure 11, and expressed as follows:

$$T_{min,bat} = f(U_{bat} \cdot I_{min}, \omega_{\text{motor}})$$
$$T_{max,bat} = f(U_{bat} \cdot I_{max}, \omega_{\text{motor}})$$

With I_{min} the minimum battery current in A, I_{max} the maximum battery current in A, U_{bat} the battery voltage in V and ω_{motor} the motor speed in rev/min.

The map-based model takes into account the E-motor efficiency, which is not constant, but depend on the E-motor speed.

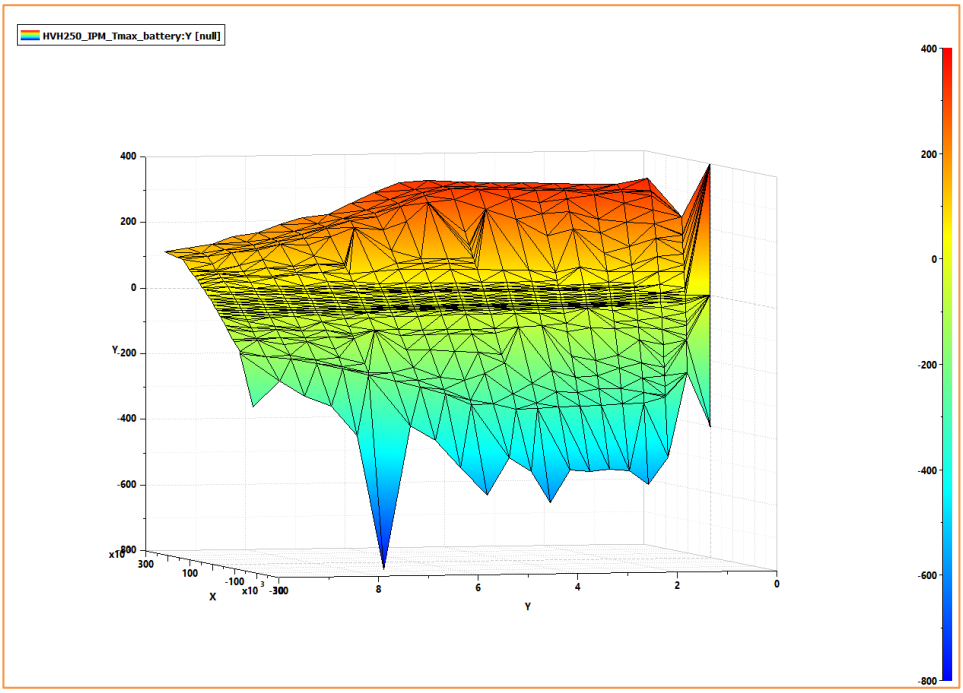

Figure 11: Maximum torque function of the available battery power & E-motor speed

1.1.4 POWERTRAIN COOLING SYSTEM

The cooling system is composed of several cooling loops and thermal inertias of different electric components as illustrated in Figure 12. The powertrain losses are split into 2 parts:

- E-motor loss
- Inverter loss

The motor is composed of inner part mainly in copper and a casing in contact with ambient. Same approach has also been applied to the inverter. The motor is not directly exchanging heat with the coolant, but heat is transferred firstly to an oil circuit for safety and lubrication purposes. An oil cooler is used to transfer the heat from oil circuit to the coolant circuit. Electric power consumption of the several pumps is also considered in the LV circuit. Several levels of battery cooling are exposed but will be detailed in section 1.3.1.

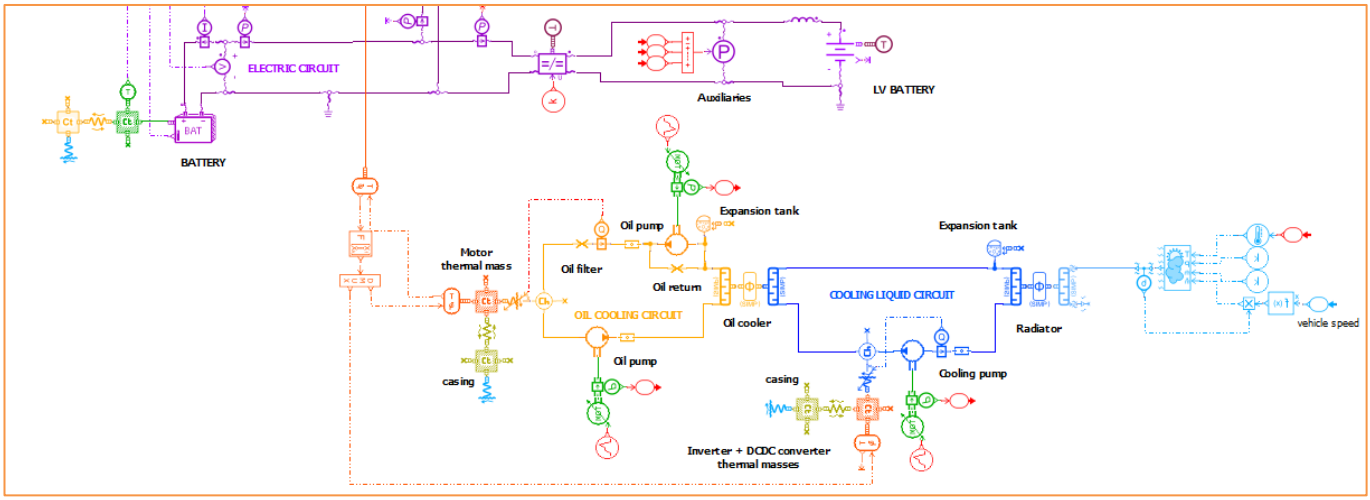

Figure 12: Cooling system

Thermal behaviour of motor and inverter are different. Indeed, the motor has slower dynamics due to higher weight, but the inverter inner temperature has faster dynamics, because inner part is much lighter in comparison to the overall inverter mass. The temperature change in degC is expressed as follow:

$$\frac{dT}{dt} = \frac{\Sigma \phi_i}{m \cdot cp}$$

With ϕ_i the different transferred heat fluxes in W, m the mass of the thermal inertia in kg and cp the specific heat of the thermal inertia in J/kg/DegC. The inner part of electric component is mainly composed of copper and the casing is of aluminium.

The parameters of the powertrain thermal modelling are detailed in Table 6.

Table 6: Powertrain thermal model parameters

Vehicle parameters	Value	Units
Powertrain loss distribution to motor	55	%
Inner motor mass	35	kg
Motor casing mass	15	kg
Inner inverter mass	0.2	kg
Inverter casing mass	9.8	kg

The conductive heat exchange in W is expressed as follows:

$$\Phi_{cond} = h_{cond} \cdot S \cdot (T_{in} - T_{casing})$$

With h_{cond} the thermal contact conductance in W/m^2/degC, S the contact surface area in m^2 and T_{in}& $\mathrm{T_{casing}}$ respectively the inner and the casing temperature in DegC.

The convective heat exchange in W is expressed as follows:

$$\Phi_{conv} = h_{conv,i} \cdot S \cdot (T_{mass} - T_{cool,i})$$

With $h_{conv,i}$ the convective heat exchange coefficient either with ambient air or with fluid in W/m^2/degC, S the contact in m^2 and T_{mass}& $\mathrm{T_{cool,i}}$ respectively the thermal capacity and the fluid temperatures in DegC.

The parameters of the different heat exchanges are detailed in Table 7.

Table 7: Thermal heat exchange parameters

Vehicle parameters	Value	Units
Thermal contact conductance in motor	20	W/m^2/°C
Thermal contact surface in motor	0.1	m^2
Thermal contact conductance in inverter	20	W/m^2/°C
Thermal contact surface in inverter	0.1	m^2
Convective heat exchange coefficient between motor and ambient	20	W/m^2/°C
Heat exchange area between motor and ambient	0.1	m^2
Convective heat exchange coefficient between motor and oil	$(Q_{oil} + 0.1) \cdot 200$	W/m^2/°C
Heat exchange area between motor and oil	0.1	m^2
Convective heat exchange coefficient between inverter and ambient	20	W/m^2/°C
Heat exchange area between inverter and ambient	0.4	m^2
Convective heat exchange coefficient between inverter and coolant	$(Q_{cool} + 0.1) \cdot 100$	W/m^2/°C
Heat exchange area between inverter and coolant	0.1	m^2

Functional models of pumps are used to produce a volumetric flow rate in L/min function of rotary speed in rev/min, as expressed as follows:

$$Q = displ \cdot \omega$$

With $displ$ the displacement of the pump in cc/min, ω the pump speed in rev/min.

The parameters of the different pumps are detailed in Table 8.

Table 8: Pumps parameters

Vehicle parameters	Value	Units
Primary oil pump displacement	10	cc/rev
Secondary oil pump displacement	5	cc/rev
Coolant pump displacement	10	cc/rev

The heat exchangers are modelled with constant thermal effectiveness to calculate the heat flux in W, as expressed as follow:

$$\phi_{HX} = \epsilon \cdot \min(m_i \cdot cp_i) \cdot \Delta T_{Max}$$

With ϵ the thermal effectiveness of the heat exchanger, m_i & cp_i respectively the mass in kg and the specific heat in J/kg/DegC of the fluid *i*.

The parameters of the different heat exchangers are detailed in Table 9.

Table 9: Heat exchangers parameters

Vehicle parameters	Value	Units
Oil cooler oil volume	0.5	L
Oil cooler oil cross sectional area	100	mm^2
Oil cooler oil flow coefficient	0.7	-
Oil cooler coolant volume	0.5	L
Oil cooler coolant cross sectional area	100	mm^2
Oil cooler coolant flow coefficient	0.7	
Radiator coolant volume	0.5	L
Radiator coolant cross sectional area	100	mm^2
Radiator coolant flow coefficient	0.7	

An expansion tank is integrated in the cooling loop to control the pressure in the circuit. In the tank, the pressure is considered as equal between fluid and air. Four interacting physical variables are calculated in this component:

- Pressure p in BarA
- Liquid temperature T_l in degC
- Gas temperature T_g in degC
- Volume of gas V_g in m^3

These interactions are expressed in equation as follows:

$$\begin{bmatrix} \frac{1}{p} & -\frac{1}{T_g} & \frac{1}{Vg} & 0 \\ -V_g & m_g \cdot cp_g & 0 & 0 \\ \frac{1}{\beta_{T_l}} & 0 & -\frac{1}{V_l} & -\alpha_l \\ -V_l \cdot T_l \cdot \alpha_l & 0 & 0 & m_l \cdot cp_l \end{bmatrix} \cdot \begin{bmatrix} \frac{dp}{dt} \\ \frac{dT_g}{dt} \\ \frac{dV_g}{dt} \\ \frac{dT_l}{dt} \end{bmatrix} = \begin{bmatrix} \frac{dm_g}{m_g} \\ dmh_g - h_g \cdot m_g + dQ_g \\ \frac{dm_l}{m_l} \\ dmh_l - h_l \cdot dm_l + dQ_l \end{bmatrix}$$

With m_g and m_l respectively the mass of gas and liquid in kg, cp_g and cp_l respectively the specific heat of the gas and liquid in J/kg/degC, dm_g and dm_l respectively the variation of the mass flow rate of the gas and liquid in kg/s, dmh_g and dmh_l respectively the variation of the enthalpy mass flow rate of the gas and liquid in W, h_g and h_l respectively the specific enthalpy of the gas and liquid in J/kg, dQ_g and dQ_l

respectively the heat flow rate provided to gas and liquid in W, α_l the expansion coefficient of the liquid in 1/degC and β_{T_l} the isothermal bulk modulus of the liquid in barA.

The parameters of the different cooling circuit components are detailed in Table 10.

Table 10: Expansion tank parameters

Vehicle parameters	Value	Units
Oil expansion tank total volume	1.5	L
Oil expansion tank gas volume	1	L
Coolant expansion tank total volume	1.5	L
Coolant expansion tank gas volume	1	L

A pressure p in bar and a temperature T in degC of the liquid in the piping & heat exchanger are computed and their interactions are expressed as follows:

$$\begin{bmatrix} 1 & -\beta_T \cdot \alpha \\ -\frac{\alpha T}{\rho \cdot cp} & 1 \end{bmatrix} \cdot \begin{bmatrix} \frac{dp}{dt} \\ \frac{dT}{dt} \end{bmatrix} = \begin{bmatrix} \frac{\beta_T \cdot \Sigma dm_i}{\rho V} \\ \frac{\Sigma dmh_i - h \cdot \Sigma dm_i + dQ}{\rho \cdot cp \cdot V} \end{bmatrix}$$

With cp the specific heat J/kg/degC, Σdm_i the variation of the mass flow rate in kg/s, Σdmh_i the variation of the enthalpy mass flow rate in W, h the specific enthalpy in J/kg, dQ the heat flow rate provided to liquid in W, α the expansion coefficient in 1/degC, β_T the isothermal bulk modulus in barA and V the volume of liquid in m^3.

The mass flow rate dm in kg/s and the enthalpy mass flow rate dmh in W are computed from the pipe cross sectional area and pressure loss expresses as follows:

$$dm = \rho \cdot C_q \cdot A \cdot \sqrt{\frac{\Delta P}{\rho}}$$

$$dmh = dm \cdot h(P_{up}, T_{up})$$

With ρ the density of the coolant in kg/m^3, A the cross-sectional area of the pipe in m^2, ΔP the pressure loss in bar, Cq the flow coefficient[3] and $h(P_{up}, T_{up})$ the specific enthalpy considered at upstream condition in kg/m^3.

The parameters of the piping are detailed in Table 11.

Table 11: Piping parameters

Vehicle parameters	Value	Units
Internal motor oil volume	1	L
Oil pipe volume	0.05	L
Oil pipe cross-sectional area	10	mm^2
Oil pipe flow coefficient	0.7	
Internal inverter coolant volume	1	L
Coolant pipe volume	0.15	L
Coolant pipe cross-sectional area	10	mm^2
Coolant pipe flow coefficient	0.7	

Finally, the radiator is cooled by air flowing from ambient under the hood. the air mass flow rate is calculated based on an estimation of the radiator air velocity [6] as expressed below:

$$dm_{air} = \rho_{air} \cdot A_{rad} \cdot V_{rad}$$

$$V_{rad} \sim 0.15 \cdot V_{veh}$$

With ρ_{air} the density of the air in kg/m^3, A_{rad} the cross-sectional area in m^2, V_{veh} the vehicle speed in m/s

[3] A focus on this coefficient is done in the section 2.1.1 dealing with performance model analysis

1.2 MiL Vehicle thermal management test bench

After describing all subsystem and their physics, their interaction will be highlighted at first and then analysed to reach first conclusions in term of energy balance within the vehicle. Finally switching to the plant model (physical model) connected with more advanced control will follow.

1.2.1 Model description

The complete vehicle model is composed of all subsystem described previously as illustrated in Figure 13. Such a test bench allows to study all interactions between subsystems in a MiL environment.

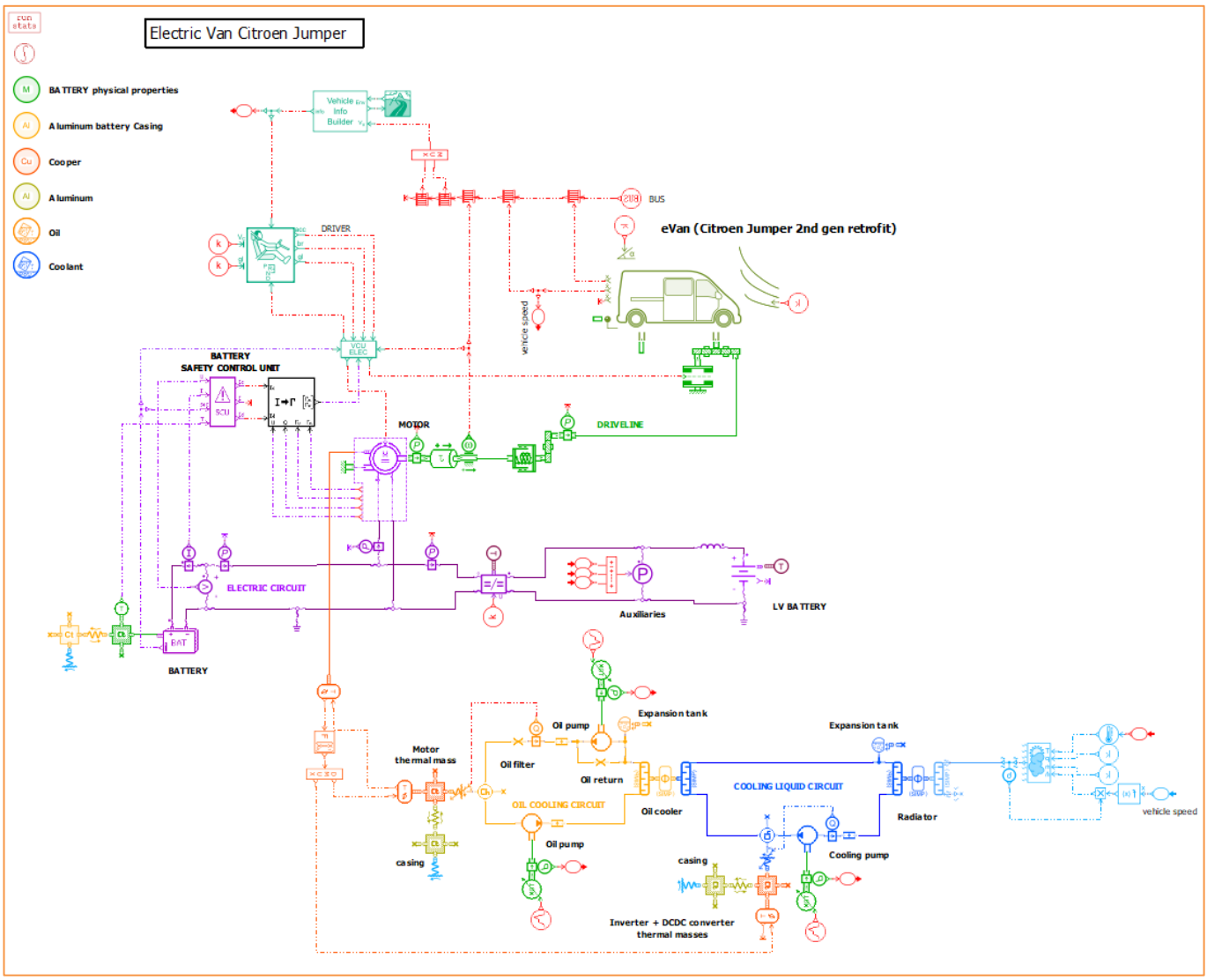

Figure 13: MiL Vehicle thermal management test bench

Main interactions are highlighted in Table 12 and described below:

- Influence of the temperature on the electric components performance
- Electric power from cooling circuit actuators (pump, fan...)
- Air flow used to cool down thermal systems under the hood

Table 12: Subsystem interactions

Interactions	Powertrain	Electric circuit	Functional control	Powertrain cooling system
Powertrain	X	-	-	-
Electric circuit	Motor power	X	-	-
Functional Control	Vehicle speed / torque request	Battery SOC	X	-
Powertrain cooling system	Motor losses / Vehicle speed	Electric consumer	Battery temperature	X

On MiL application, the virtual test bench can run on variable step solver. The main advantage is the CPU time and the ease of use, because the solver automatically selects the right solver as function of the stiffness of the system [7]. Indeed, any step size can be set and generally default settings works almost always.

1.2.2 Results and analysis

The first variables to study are those related to the powertrain performance, because this subsystem will be identical between the different models that are presented in this document. Influence of the battery modelling or control algorithms can be easily compared.

The vehicle speed is compared with control speed from standardized driving cycle. In this example the WLTC has been selected, as show in Figure 14. We observe that the vehicle speed is accurately following the control speed with maximum error of 3.5 km/h at some instances. These differences mainly occur when vehicle is stopping, due to a very functional brake model. Nevertheless, except in stopping area, the error is lower than 1 km/h, which corresponds to the accuracy we observe in speed regulator today.

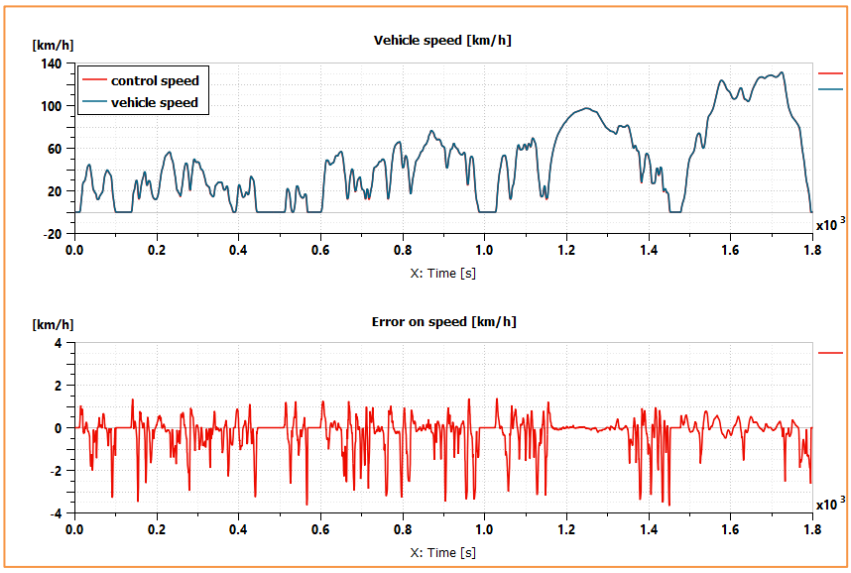

Figure 14: Vehicle speed results

The second variables to study are the battery and electric variables like the battery voltage or the current distribution. The SOC is also important to follow for safety aspect and control.

The battery voltage is evolving between 760 V and 790 V, except during the last period, where we can observe a drop to 710 V. Indeed, the battery voltage takes the internal battery resistance into account, meaning a voltage drop appears when current demand is high, as show in Figure 15.

During this WLTC driving cycle, the battery SOC decreases about 14%. Indeed, we observe that the current peaks are very low during urban and extra urban parts. Only during motorway part, current demand is high to maintain the light truck driving at 120 km/h, due to higher aerodynamics losses.

Looking at the current level, we can observe negative currents peaks at the end of the driving cycle, because during this period, we are able to load the battery during braking phase until the standstill. Indeed, the regenerative braking is active when battery SOC drops below 85%, so after 1150 s.

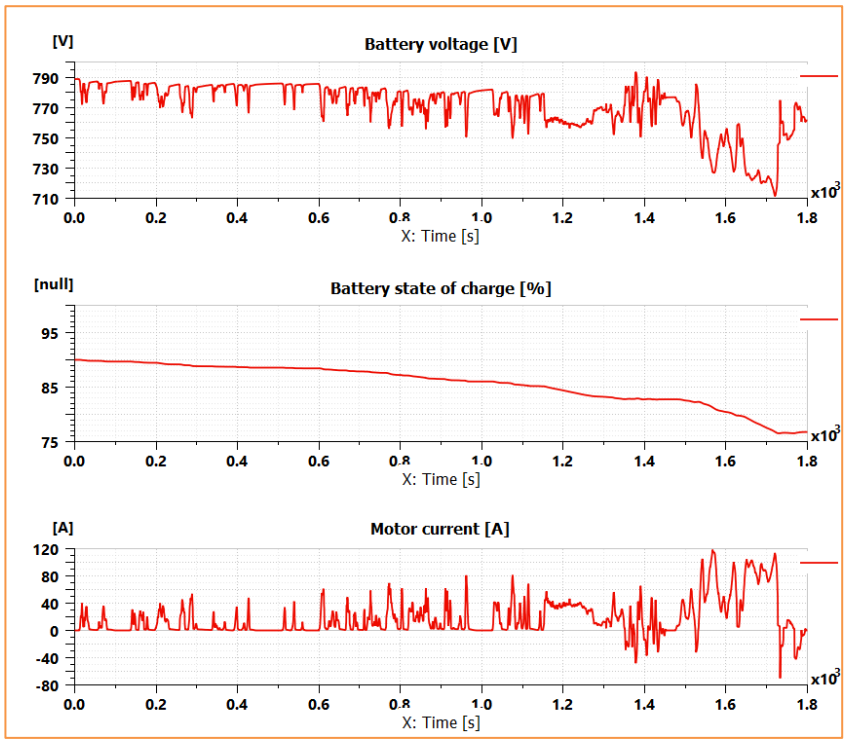

Figure 15: Electrical results

The last subsystem studied is the powertrain cooling system. Motor losses are transferred to the inverter and motor thermal masses, then the latter are cooled. Motor and inverter capacities have different thermal behaviour mainly due the weight of both electric components (35 kg for motor and 0.2 kg for inverter). The consequence is a smoother thermal behaviour for motor temperature instead of high peak of temperature in inverter.

Nevertheless, the motor temperature reaches higher values because this component is not directly cooled by coolant but by intermediate oil cooling loop as we can observe in Figure 16. Indeed, the average oil temperatures is around 5 degC higher than the coolant temperatures.

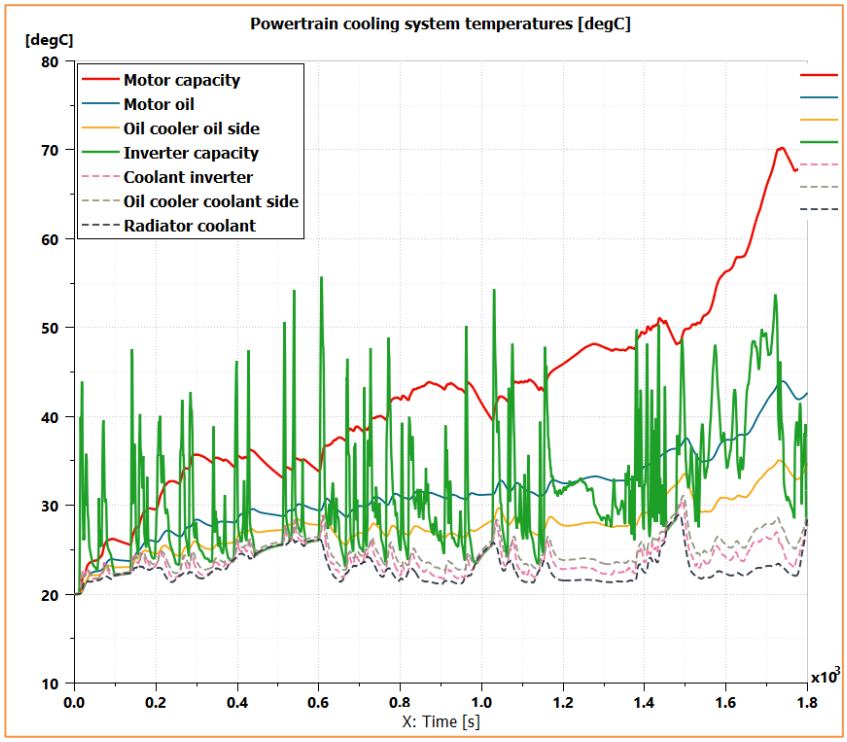

Figure 16: Thermal results

Finally, we can study the interaction of different subsystems by analysing the power distribution in the complete vehicle as shown in Figure 17. We can observe the battery power is almost identical to the motor power. Indeed, the difference corresponds to the power coming from the LV circuit, which is evolving between 20 and 40 W in comparison with the peak of 60~80 kW in motor. The consequence is the cooling of electric actuators is negligible on vehicle level. The only thermal component which has a real impact is the AC system with its 5-6 kW electric compressor.

The effective powertrain power is lower than motor power, because the latter generates heat losses. We can observe these ones are always positive whatever the mode of the motor is:

- in propulsion mode, $P_{motor} > P_{powetrain}$
- in regenerative mode, $P_{motor} < P_{powetrain}$

The heat losses are then transferred to motor and inverter masses as already discussed. We can observe that the order of magnitude of power between losses and radiator are equivalent. The main differences are in following situations:

- peak losses have been absorbed by thermal masses
- radiator is not able to absorb all power of losses during motorway period leading to an increase of temperature for motor and inverter.

The oil cooler power corresponds to the motor loss only and its trends is like the oil temperature trends with a smoother thermal behaviour.

To conclude such vehicle thermal management virtual test bench is useful particularly for:

- study the thermal transient behaviour for electric powertrain
- validate first control strategies.

In previous model, modelling of battery thermal behaviour is very limited. Therefore, a virtual test bench focusing on the battery management has been developed based on previous model. It was done simply by removing powertrain cooling system, which highlights the modularity of this approach.

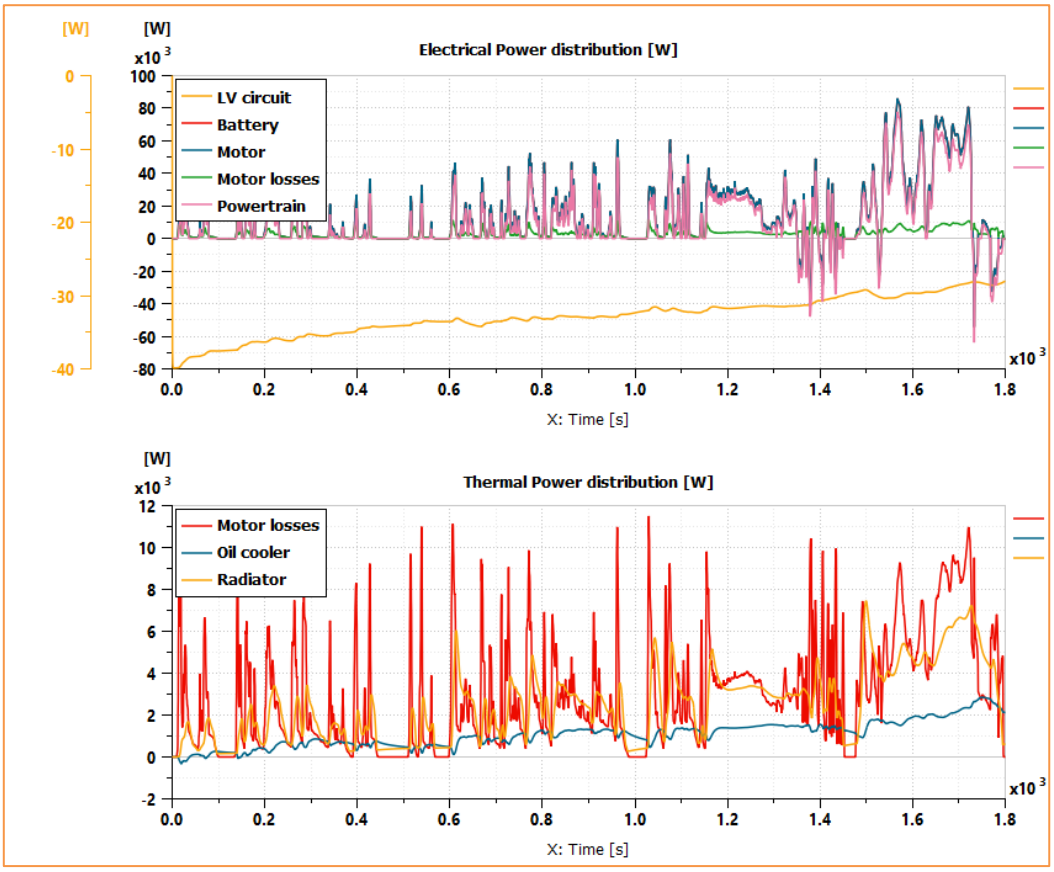

Figure 17: Power distribution results

1.3 MiL Battery Management System Test Bench

Powertrain system modelling approach has been validated with previous model. Now a focus on the battery modelling is done, especially to have a better understanding of the inner battery thermal behaviour and allow for multi temperature control.

1.3.1 Model Description

The battery management virtual test bench is based on the previously described model, except for the battery modelling as shown in Figure 18. Indeed, in this model, the battery pack is modelled with its 16 modules in series; each module is composed of cells in series and parallel as detailed in Table 13.

Table 13: Battery module architecture

Module architecture	Value	Units
Cell in series	12	-
Cell in parallel	20	-

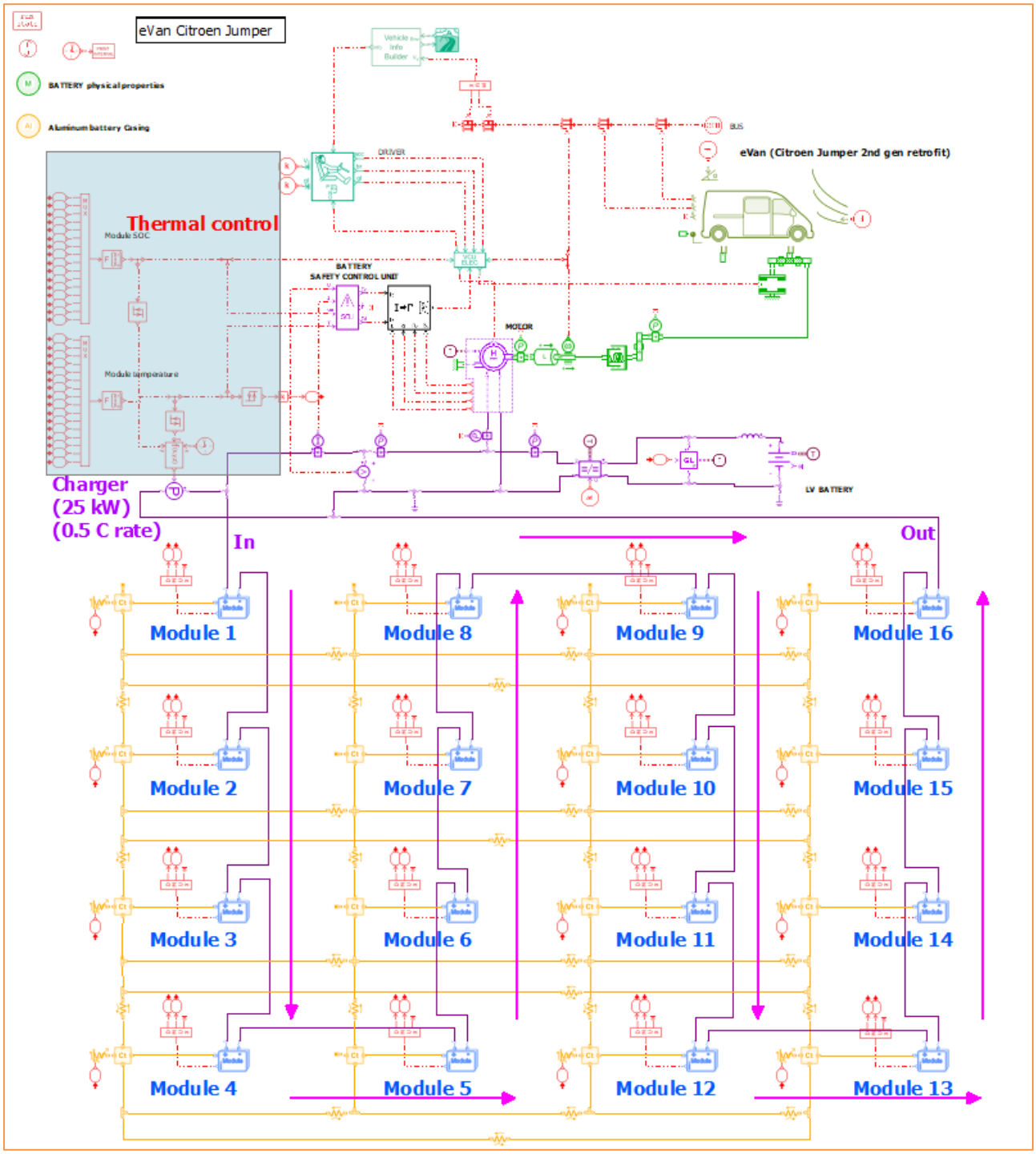

Figure 18: MiL Battery management system test bench

However, not every single cell is represented in each module of the battery pack model. To limit the number of components in the sketch, each module includes only 4 battery cell components in series. Each battery cell model is used to represent 3 groups of cells, which means 60 cells (20P3S) in total. All these 60 cells are assumed to be identical, so only one battery model is enough to represent all of them as shown in Figure 19.

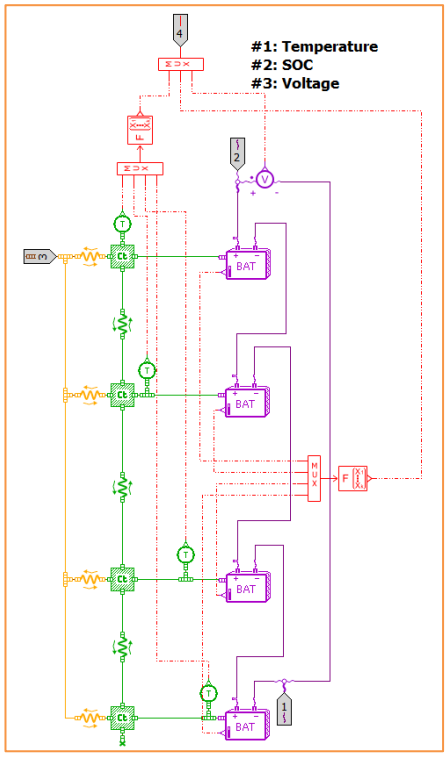

Figure 19: Battery module

By doing so, the battery pack is split into 48 battery models, which allows to have access to 48 temperatures of different places in the battery pack. The battery pack casing is also modelled. The casing is divided into 16 parts and each part is represented by a thermal mass element. The thermal mass of each part of the casing is connected to the nearby module, as explained in Figure 20.

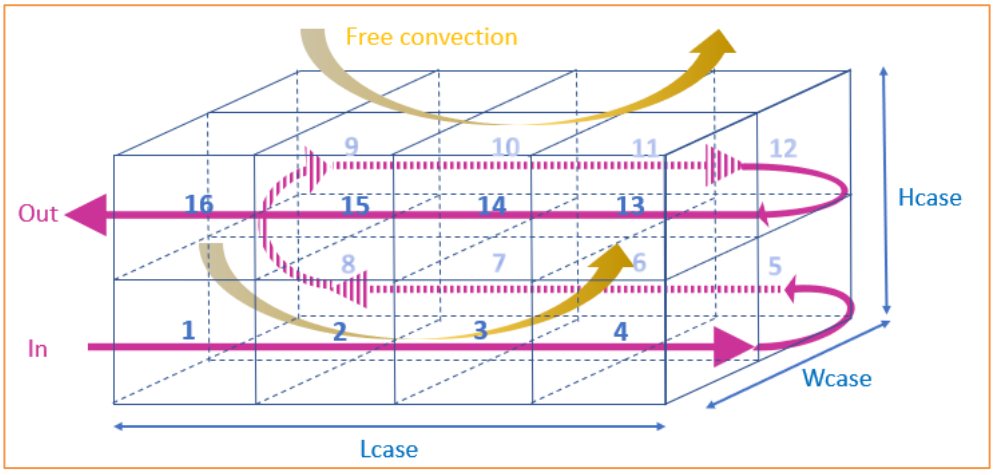

Figure 20: Module connection and casing architecture

Free convection is considered only for 2 surfaces of the casing to highlight the temperature gradient within the battery pack. As already mentioned, the values given below are not the real ones because of the confidentiality reasons.

The parameters of the different heat exchanges are detailed in Table 14.

Table 14: Thermal heat exchange in battery pack parameters

Vehicle parameters	Value	Units
Casing length	1000	mm
Casing height	500	mm
Casing width	800	mm
Casing thickness	5	mm
Free convective heat exchange coefficient between casing and ambient	20	W/m^2/°C
Forced convective heat exchange coefficient between casing and ambient	200	W/m^2/°C
thermal contact conductance between battery casing and cells	20	W/m^2/°C

1.3.2 RESULTS AND ANALYSIS

To illustrate the use of the battery pack model with a BMS, a case study to compare the electro-thermal behaviour of the battery pack under 2 cooling scenarios has been defined: with and without active air cooling.

For the scenario with active air cooling, the following strategy is applied:

Active cooling **on** $if\ T_{bat,max} > 35\ degC$
Active cooling **off** $if\ T_{bat,min} < 30\ degC$

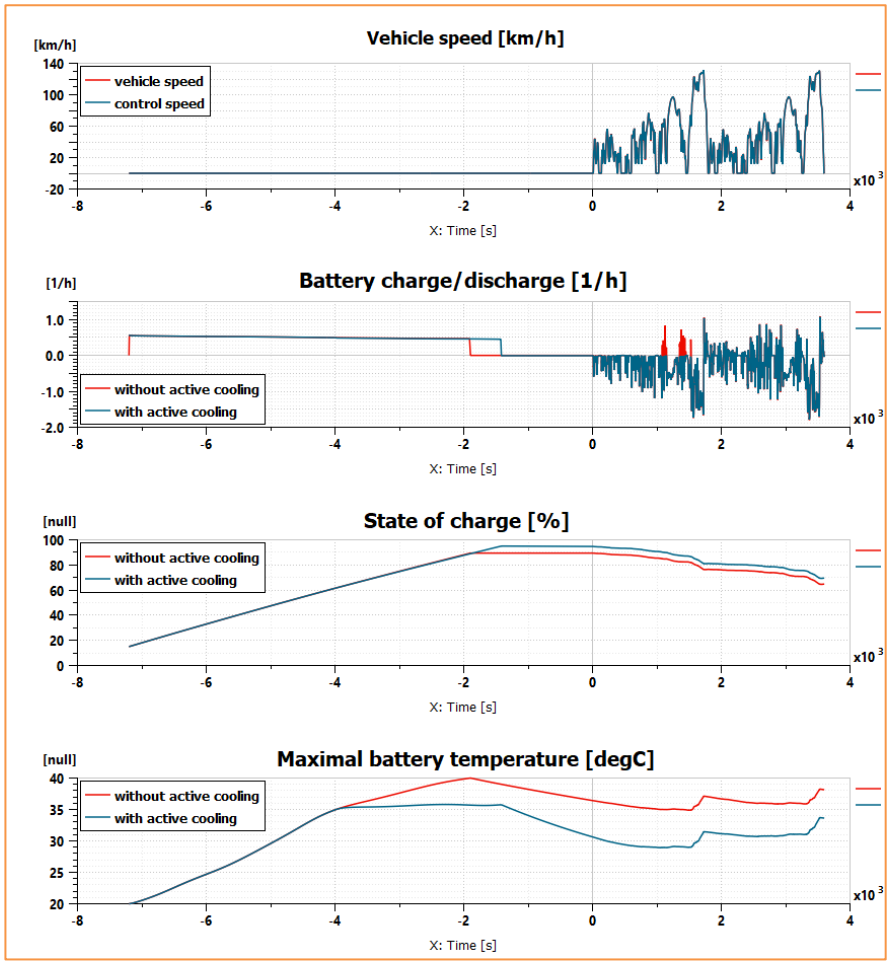

Figure 21: Cooling comparison results

For both scenarios, the battery pack is charged during the first 2 hours with functional charger of 25 kW (corresponding to a 0.5 C rate). Then the vehicle follows 2 WLTP driving cycles. The comparison of the simulation results for the 2 scenarios shows that the active cooling helps to increase the effective charge time and to decrease significantly the battery cell temperatures as shown in Figure 21.

Indeed, higher state of charge is reached with active cooling because the charge is stopped during less time. Without active cooling maximal battery temperature reaches 45 degC, forcing the charger to stop, which is not the case with active cooling.

About the charge of the battery during the driving cycle, we observe a start of regenerative braking sooner without active cooling around 500 s, because the state of charge decreases until 85% sooner, as mentioned in the vehicle control unit component.

The battery temperature distribution is slightly different between both scenarios, as shown in Figure 22. Indeed, the two scenarios can clearly be distinguished; module directly cooled down and module indirectly (through conduction) cooled down by convection. With active cooling, the average temperature level is lower, but a higher spread (0.4 degC instead of 0.1 degC). The reason is that the heat exchange surface is different for each module. So convective heat exchange is not homogenous. To obtain more overall homogenous temperature distribution, a cooling with liquid throughout the pack is recommended, as studied in WP5 [8].

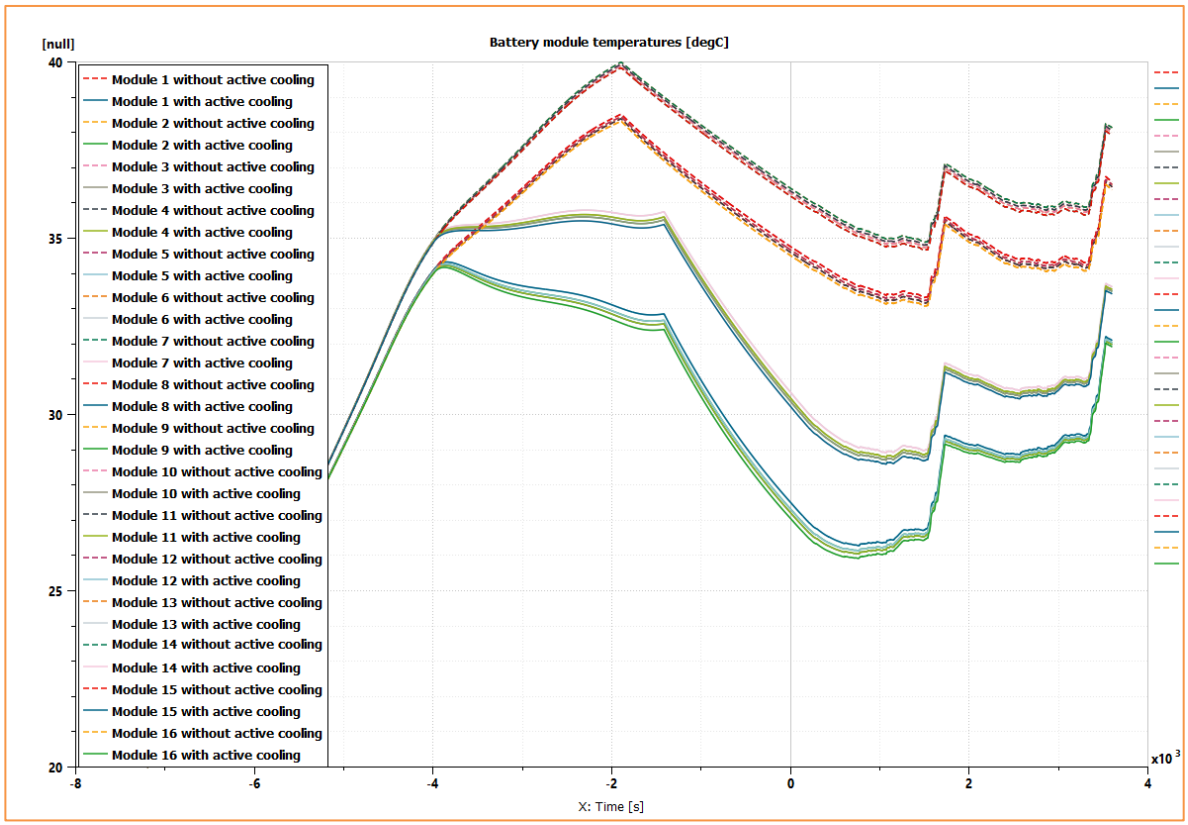

Figure 22: Temperature distribution results

To conclude, this model, with extended battery detail, will be used in SiL and HiL environment to compare different control strategies. Thanks to this multi temperature and voltage access, this model will be also connected with the real hardware developed by Lion Smart in WP6 [9].

2 SiL VIRTUAL TEST BENCH

2.1 Co-SIMULATION & REAL TIME CAPABILITY

To use the battery pack model for SiL and HiL tests, the simulation time of the battery pack model must be analysed to confirm its real time capability. Indeed, a model in SiL platform and especially in HiL platform must be run with fixed step solver and must be faster than real time at each integration step.

2.1.1 PERFORMANCE MODEL ANALYSIS

Thanks to an embedded analysis tool in Simcenter Amesim, we can study the performance of the model, especially with automatic linear analysis along the simulation, as shown Figure 23. The main interest is to detect the maximum frequencies of the system and when these ones occur. Furthermore, the contribution of states variables is listed for each frequency (top contribution table). So, model reduction methodology becomes easier and faster.

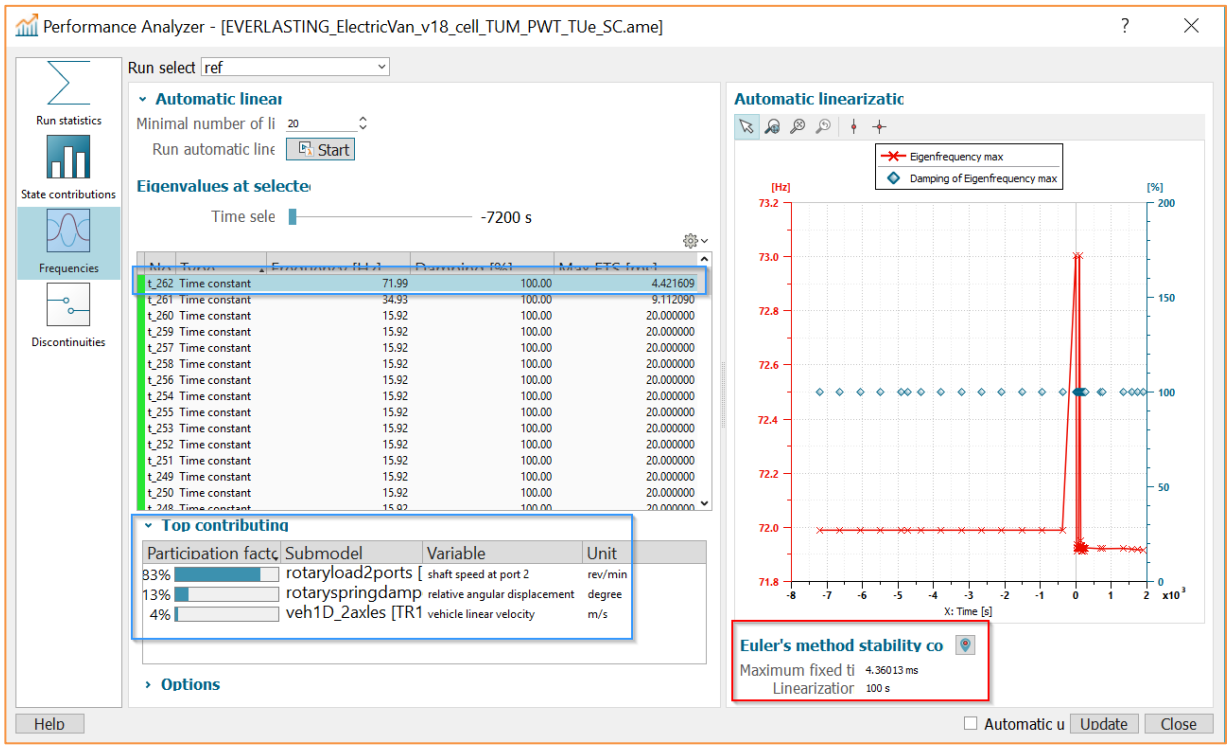

Figure 23: Performance model analysis

In this model, we observe the maximal frequency is linked to the mechanical part of the model, between motor shaft speed and vehicle speed. The value of this frequency is around 73 Hz at maximum. So, the maximum integration step is 4.3 ms, as expressed by the Euler criteria below:

$$\delta t_{stability} = \frac{2}{2 \cdot \pi \cdot f_{max}}$$

$$\delta t_{accuracy} = \frac{1}{2 \cdot \pi \cdot f_{max}}$$

With f_{max} the maximum frequency of the system in Hz.

In the model an integration step has been set at 2 ms to ensure stability all the time.

2.1.2 RESULTS

Figure 24 shows an analysis of the simulation time for the scenario with active air cooling. The simulation was run with a fixed step solver by setting the integration time step to 0.002 s. The simulation was carried out on a laptop with Intel i7 2.6 GHz CPU, 16 GB RAM. The cumulative CPU time for the simulation is 740 s at the end of the simulation, which is 14.6 times faster than the duration of the scenario (10800 s). The mean CPU time used per step (0.1 ms) is then 14.6 times faster than the fixed time step value (2 ms). The real-time capability of the Battery Management System test bench is then validated.

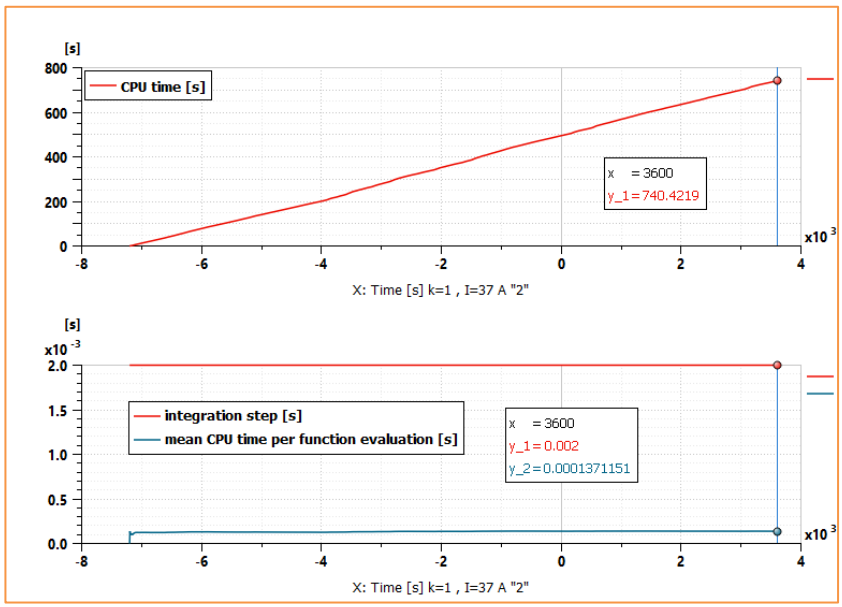

Figure 24: Simulation time with fixed step solver

2.2 VIRTUAL TEST BENCH INTERFACE

After validating the virtual test bench on MiL application for BMS control and ensuring the SiL & HiL compatibility in terms of solver and CPU time, a focus was directed towards more complex BMS functions. With access of several cell temperatures and voltages, the objective is to test the cell balancing strategies by adding a small converter in parallel of each battery module to limit the voltage disparity.

2.2.1 CELL BALANCING

For each module, its voltage is compared with the mean value from the 16 modules. A command is then sent to the converter, as shown in Figure 25, to generate a current to reduce the voltage gap, expressed as follows:

$$U_{mod} - \bar{U} > 0.1\,V \rightarrow I_{conv} = 8\,A$$
$$U_{mod} - \bar{U} < -0.1\,V \rightarrow I_{conv} = 8\,A$$

With $\bar{U}$ the mean voltage in V.

The converter is connected:

- from one side to the module I/O
- from other side to the battery pack I/O

Furthermore, the converter is not perfect and an efficiency of 0.75 has been considered, meaning during cell balancing converter heat loss is transferred to the casing in contact of the corresponding module.

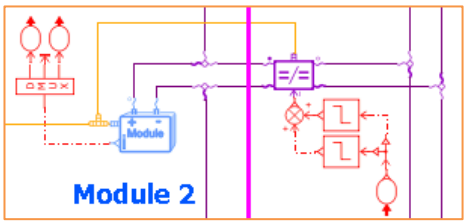

Figure 25: Cell balancing

2.2.2 INTERFACE

In battery cell model, SOC is continuously calculated, but to be more realistic with real BMS, this one is not used as BMS input. Instead, SOC is calculated based on battery current modulated by the cell balancing current. Details of the control function are given in the section 2.3. Nevertheless, module temperature and voltage are used as normal signals and transferred to the BMS, which is developed with Matlab/Simulink, illustrated with the interface in Figure 26. Additionally, to these signals, the battery current is also measured.

The BMS has 3 mains functions:

- Thermal control
- Charging control
- Cell balancing

Additional information like min/max SOC and min/max temperature are also available to centralize all main information in the Simcenter Amesim model for easier post-processing.

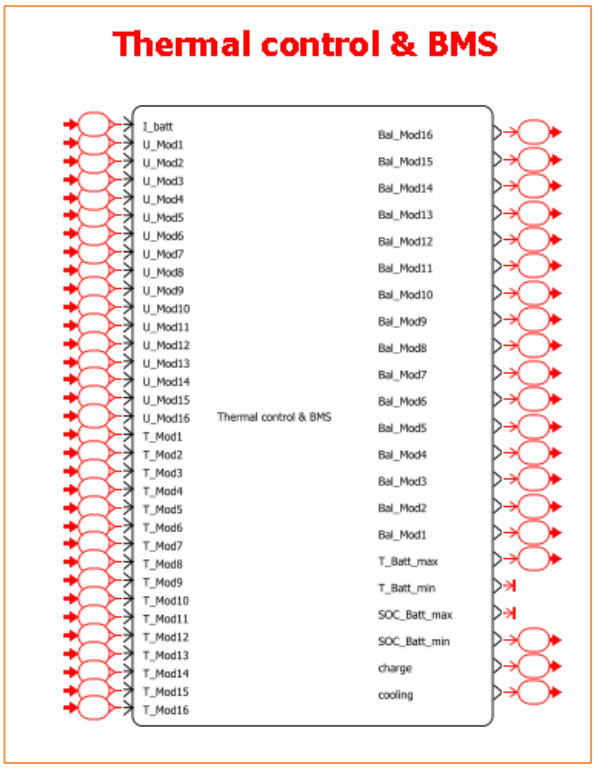

Figure 26: BMS control interface

2.2.3 MODEL DESCRIPTION

The complete plant model developed with Simcenter Amesim is very similar to the MiL BMS test bench, except the control, which is now more complex with several functions, as shown in Figure 28. This plant model runs also at a fixed time step with same integration step set at 2 ms with an Euler method, as shown in Figure 27.

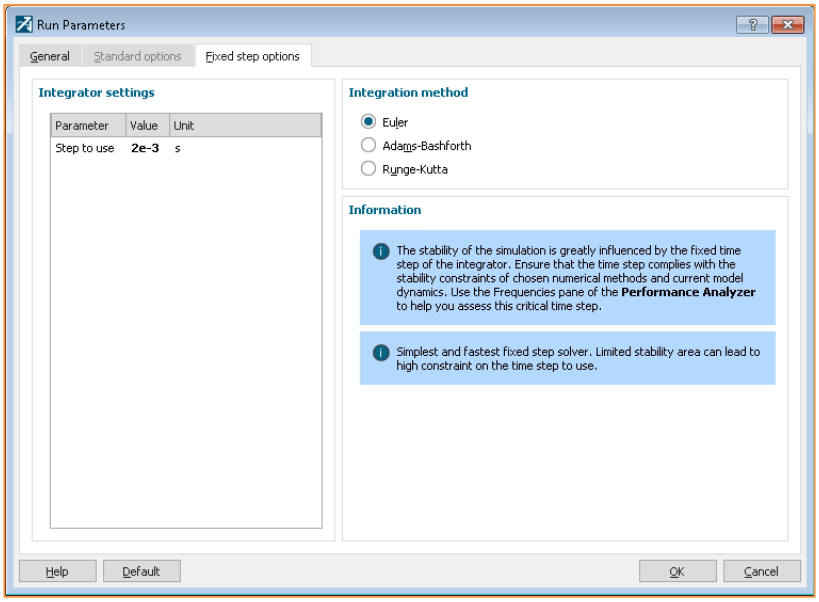

Figure 27: SiL plant model solver settings

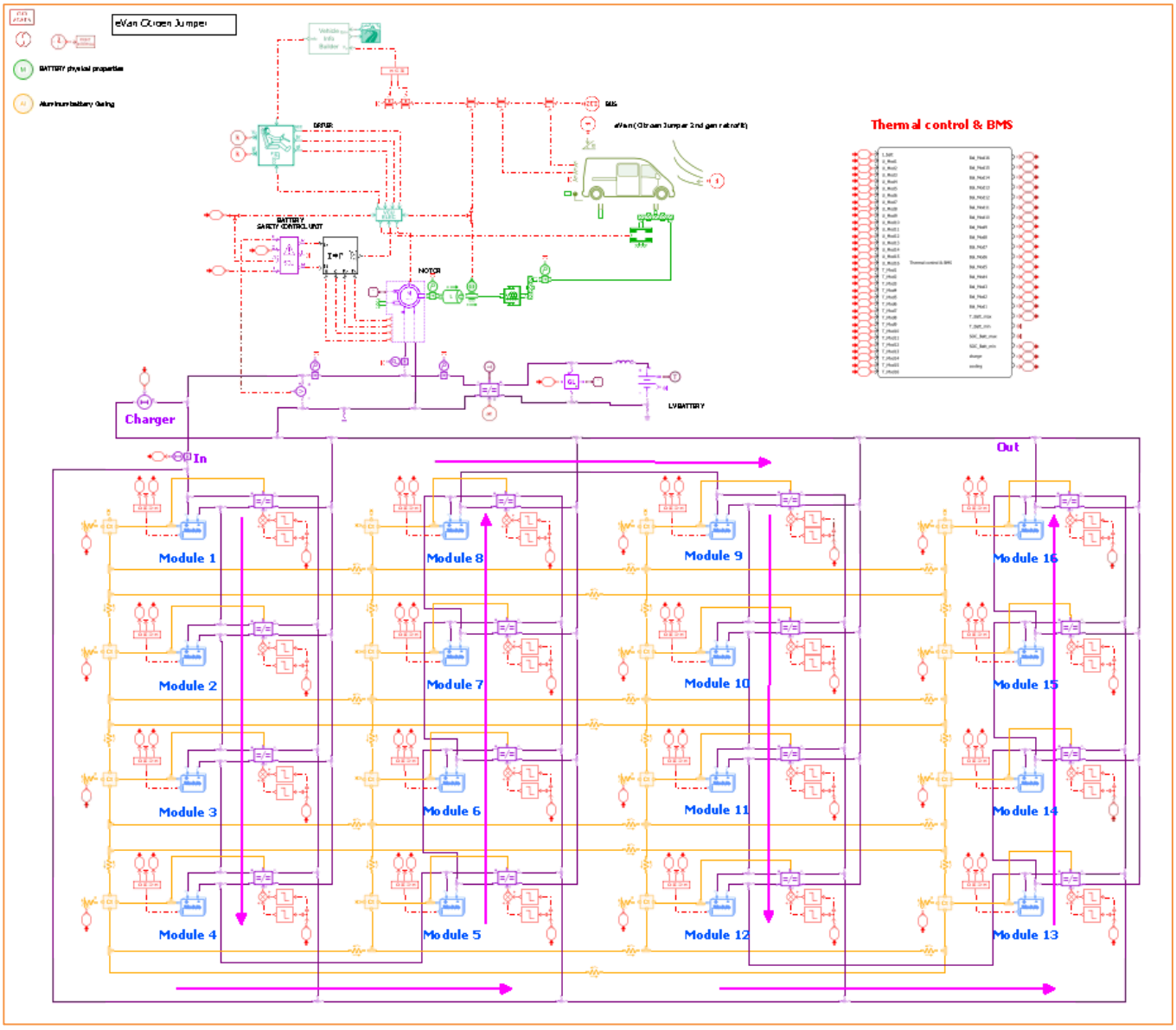

Figure 28: SiL Battery management system test bench (plant part)

2.3 MATLAB/SIMULINK COSIMULATION

The BMS is now developed with MATLAB/Simulink to prepare final HiL co-simulation. BMS functions are still functional ones but highlight what can be calculated in a BMS thanks to measured data from model or real battery.

The version of MATLAB used in this SiL test bench is a MATLAB 2016b 64 bits.

2.3.1 BMS ARCHITECTURE

As already mentioned, three functions have been developed in this BMS, as shown in Figure 29:

- Thermal control
- Charging control
- Cell balancing

The thermal function is the same as the one developed in Simcenter Amesim for the MiL test bench (see section 1.3.2 for details).

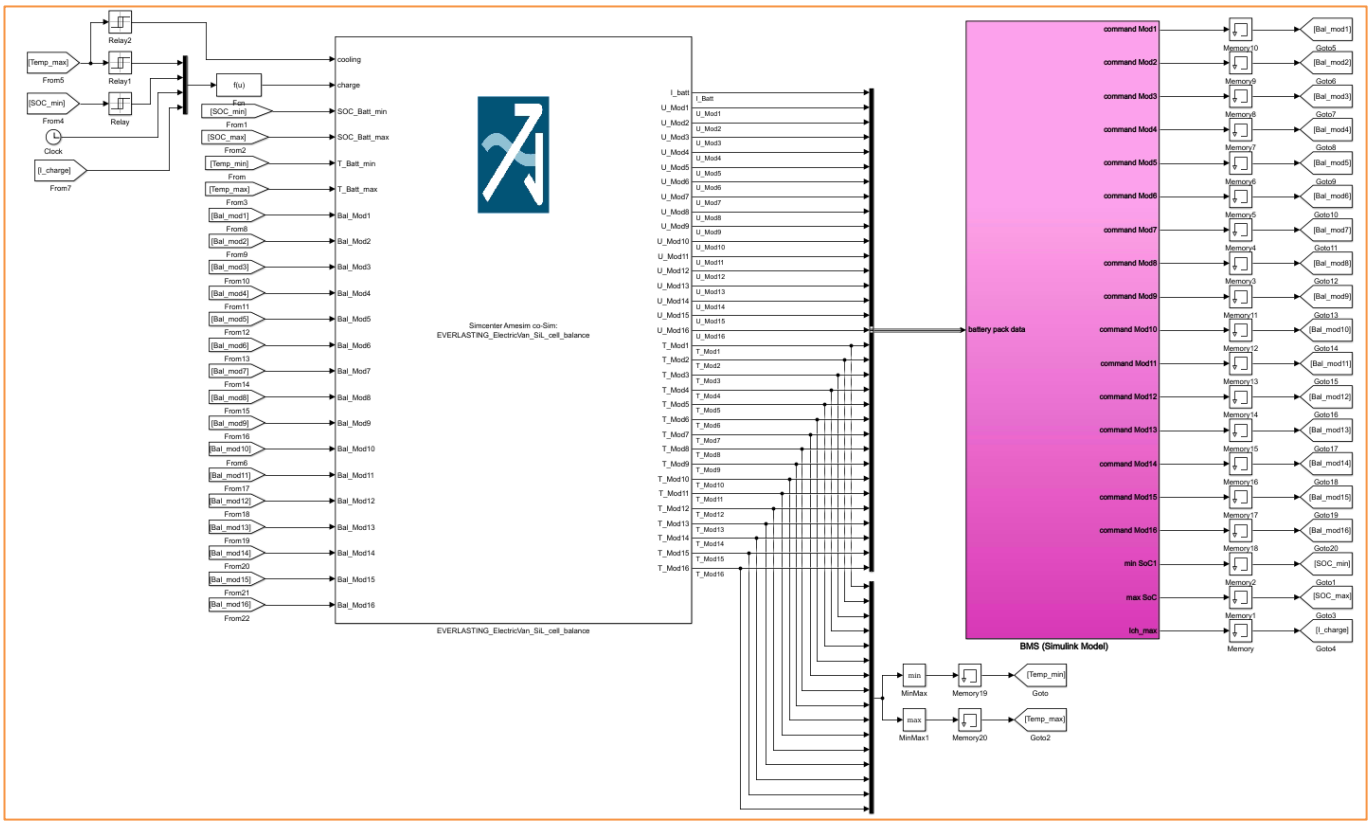

Figure 29: SiL Battery management system test bench (control part)

In the BMS block there are the SOC estimation for each module and the charge control, as shown in Figure 30. The maximum and minimum SOC are calculated in this block. There are 3 blocks:

- the green box corresponds to the charge control
- the yellow box the balancing decision for each module
- the blue box the SOC estimation for each module.

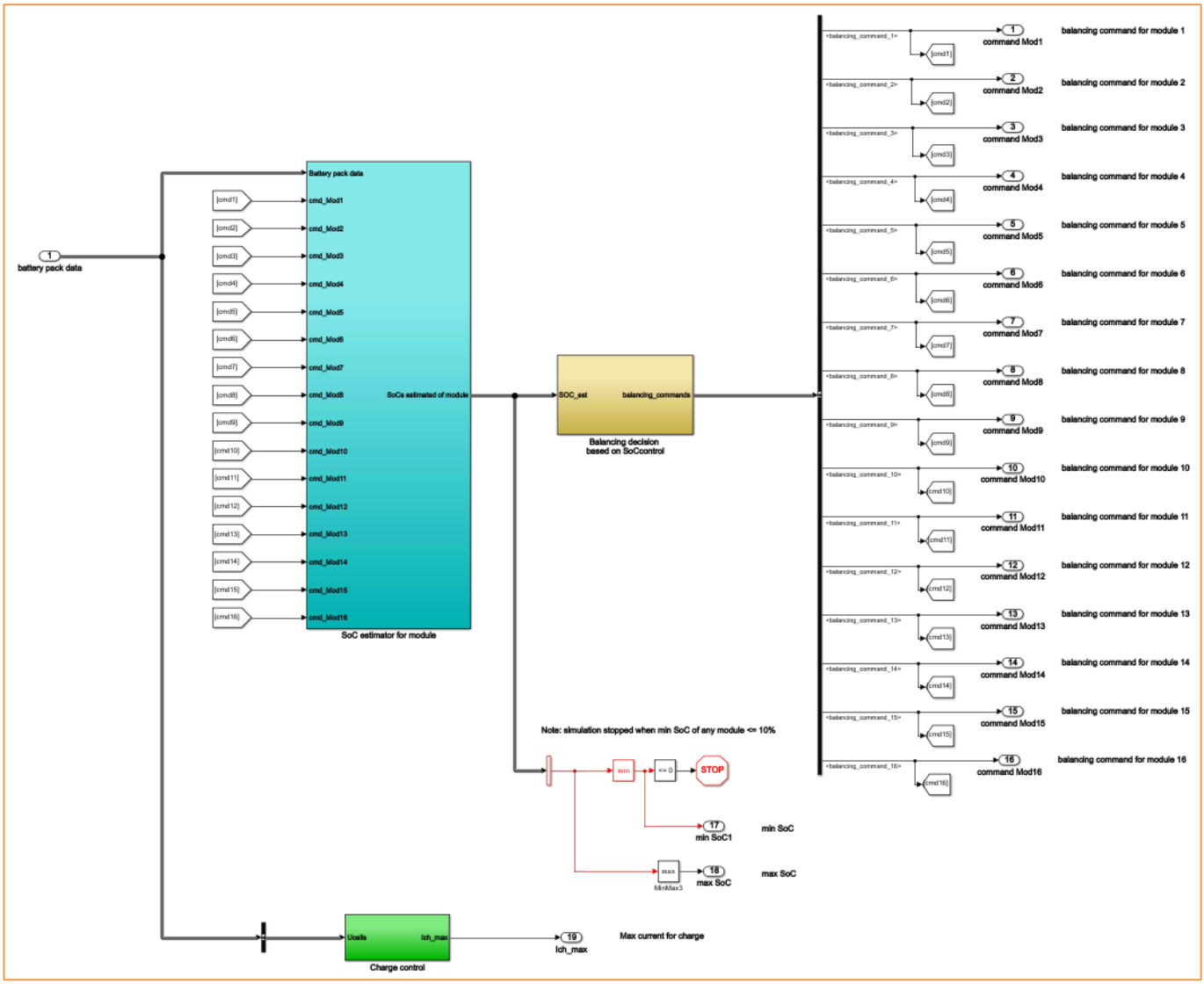

Figure 30: BMS block

2.3.2 SOC ESTIMATOR

The SOC is not a battery variable which can be measured. So, it must be estimated by the BMS. Furthermore, the cell resistance and the capacity of the module are also calculated, as shown in Figure 31. The SOC is directly calculated from the module capacity and the module current, meaning the balancing current is considered for each module. The equation is the same as expressed in section 1.1.2.

The module capacity is just the product of the nominal capacity multiplied by the number of cell in parallel in the module, so 20.

The resistance of the module depends on the SOC and the temperature and at top of it is function of the mode: either charge, or discharge.

We can observe additional calculation in Figure 31, but they are inactive, because we considered the quasi-static SOC estimation only a function of the current and not the diffusion of the cell (transient effect).

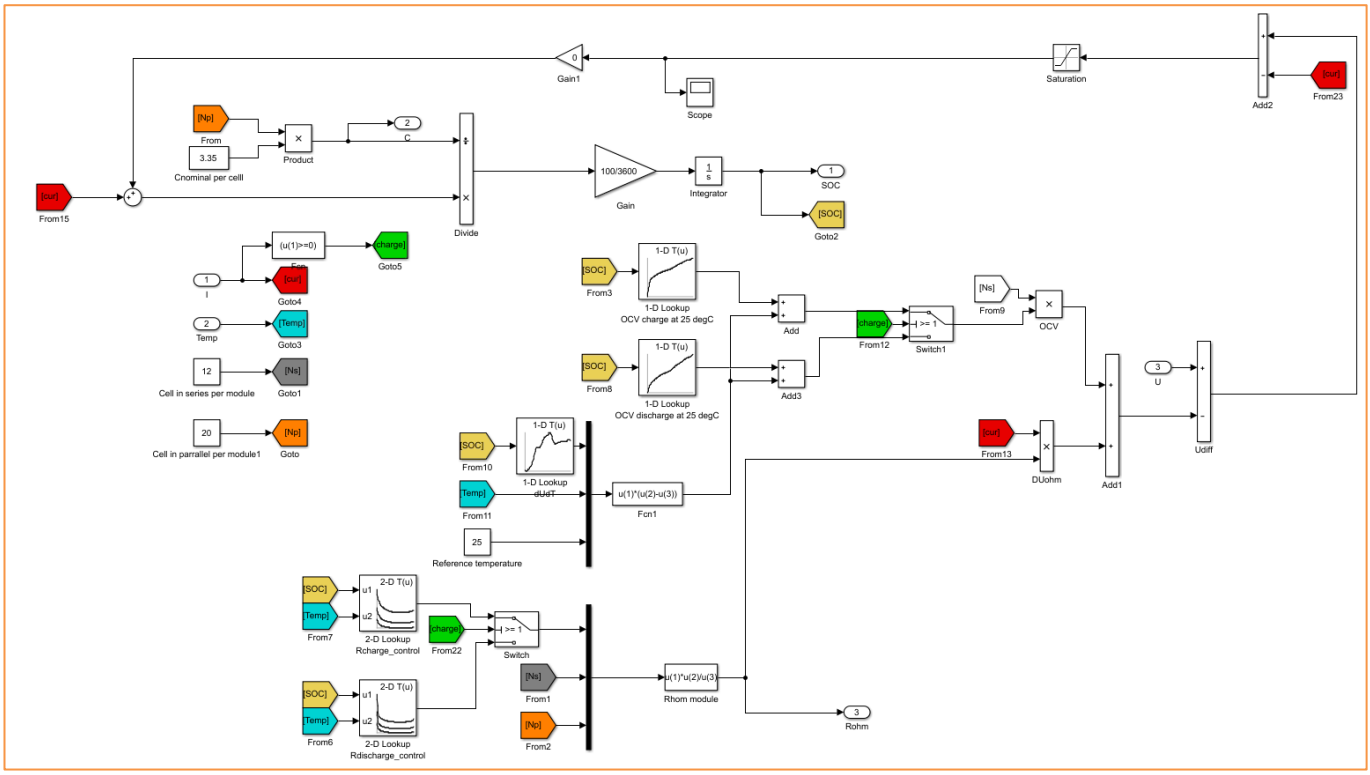

Figure 31: BMS SOC estimator

2.3.3 CHARGE CONTROL

For the charging control, same SOC thresholds have been applied. Indeed, in the MiL test bench, a constant electric power has been applied, meaning charging current was dependent on the battery voltage. In the SiL test bench, a current is directly applied, and this time is controlled based on maximum cells voltage, as shown in Figure 32.

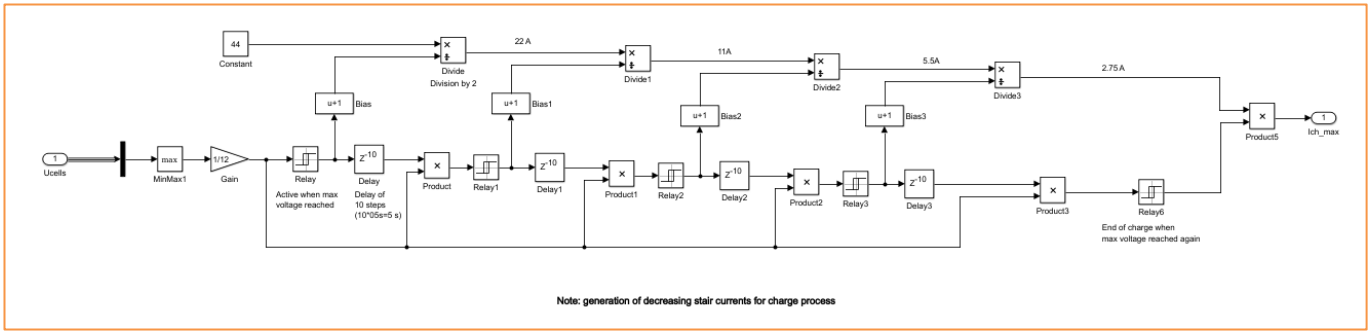

Figure 32: Maximum charging current available

Until the cells voltage is lower than 4.2 V, the maximum current is applied (44 A). Then a delay of 5 s is applied before starting current charge decrease. This process is done 4 times before switching off the charge, as expressed below:

$$U_{cell,max} < 4.2\ V \rightarrow I_{charge} = 44\ A$$

$$U_{cell,max} > 4.2\ V\ at\ t = t_0 \rightarrow I_{charge} = \frac{44}{2} = 22\ A$$

$$U_{cell,max} > 4.2\ V\ at\ t = t_1 = t_0 + 5\ s \rightarrow I_{charge} = \frac{22}{2} = 11\ A$$

$$U_{cell,max} > 4.2\ V\ at\ t = t_2 = t_1 + 5\ s \rightarrow I_{charge} = \frac{11}{2} = 5.5\ A$$
$$U_{cell,max} > 4.2\ V\ at\ t = t_3 = t_2 + 5\ s \rightarrow I_{charge} = \frac{5.5}{2} = 2.75\ A$$
$$U_{cell,max} > 4.2\ V\ at\ t = t_4 = t_3 + 5\ s \rightarrow I_{charge} = 0\ A$$

With $\bar{U}$ the mean voltage in V.

So, when the cell voltage achieves a threshold corresponding to the $OCV_{95\%SOC}$, the charging current is reduced to reach a low current and a cell voltage close to the $OCV_{95\%SOC}$. Indeed, with charging current, the cell voltage is not equal to the $OCV_{95\%SOC}$ due to internal resistance. By using this methodology, charging process will stop at 95% SOC.

2.4 SiL Battery Management system test bench

To validate the SiL approach, the same scenario has been applied as for the MiL virtual test bench, meaning 2 hours charging then 2 WLTC driving cycle after each other.

2.4.1 Simcenter Amesim results

The plant model of the SiL virtual test bench has been getting expected values by running properly, validating the SiL approach. Indeed, the vehicle speed is following well the driving cycle and the battery charge is correctly controlled with temperature safety measure, as shown in Figure 33. When the maximal battery module temperature reaches 40 degC at -3475 s, charge is stopped to cool down the battery before restarting when temperature drops to 35 degC.

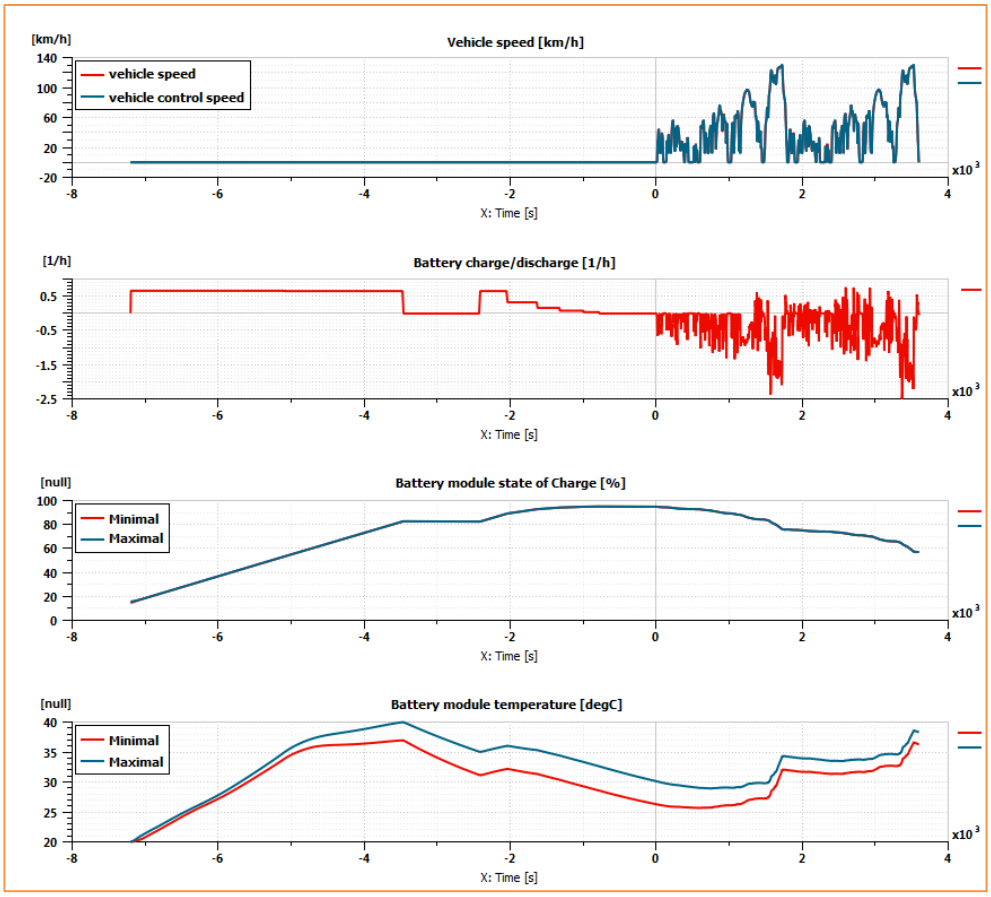

Figure 33: Simcenter Amesim SiL results

We observe at the end of the charge a reduction of the charging C-rate to achieved 95 % SOC. Indeed, limited current generates lower heat losses. By this way, battery is cooled down because heat losses are more than balanced by cooling capacity from active cooling.

Another important observation is the temperature distribution. Indeed, the temperature is quite homogenous during 1st charging period with maximal difference of 2 degC, but this difference increases with active cooling to 3.8 degC at the end of the charging period. So, cooling with liquid should be better to ensure a more homogenous temperature distribution within the battery pack.

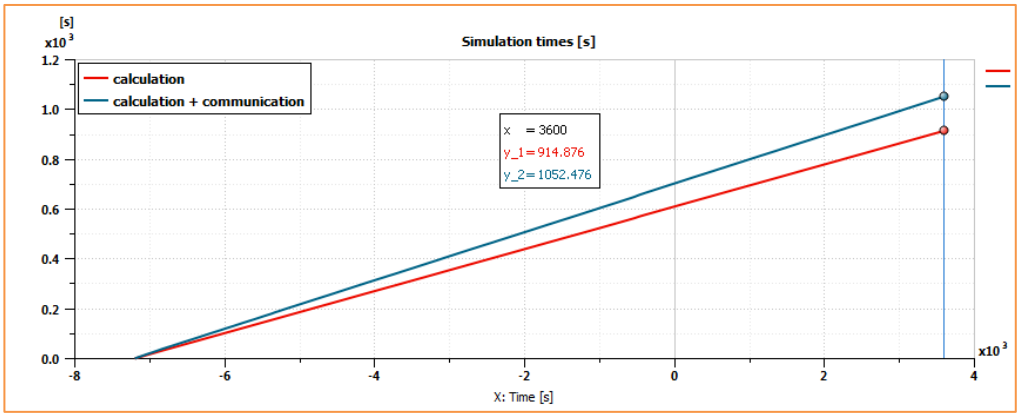

Figure 34: SiL simulation time results

The SiL virtual test bench is still complying with real-time capability even if communication time has been added to exchange variables between Simcenter Amesim and Simulink, as shown in Figure 34. The overall simulation has lasted 1050 s for 10400 s simulation time, meaning 9.9 faster than real time. We also observe that 13 % of the simulation time is used for communication between the two software's.

2.4.2 SIMULINK RESULTS

In the control model, we highlight the current distribution in each module by splitting the current from the charger and electric motor to the DC/DC converter used for balancing, as shown in Figure 35.

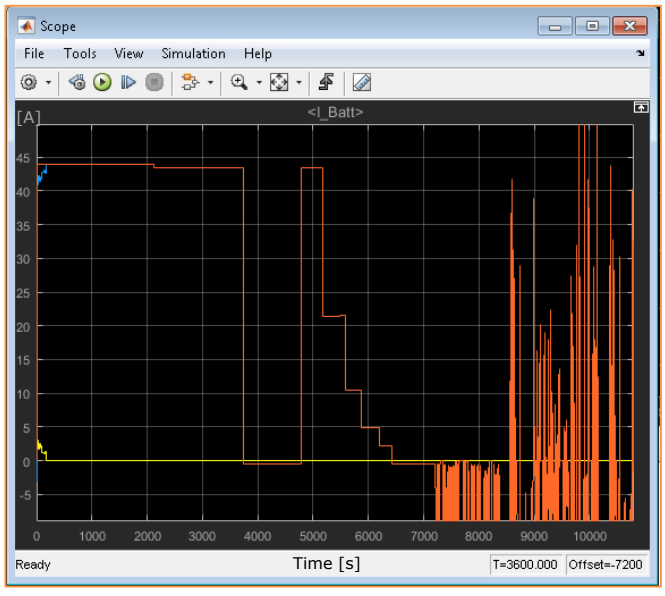

Figure 35: Influence of the balancing current on the battery current

We can observe during the 300 s the balancing current is applied, with a maximal value of 3 A at the beginning. After 150 s, the current is almost split by 2, meaning SOC distribution has been reduced and less modules must be balanced.

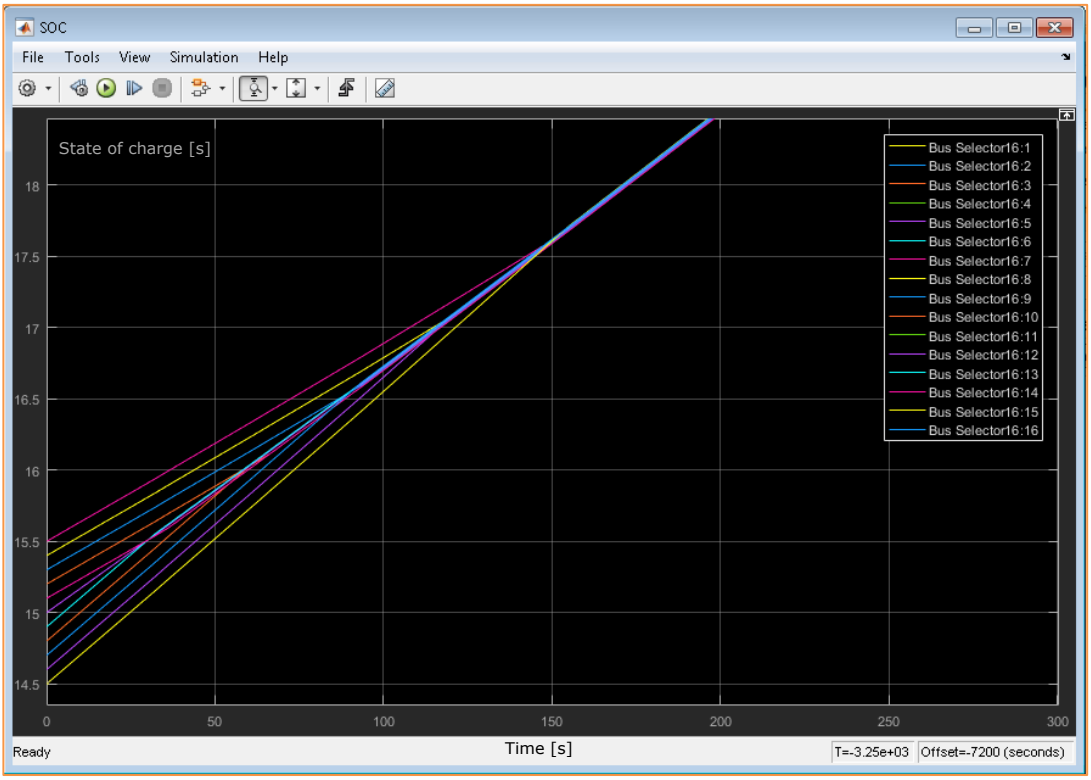

Figure 36: module SOC distribution during call balancing

During the first 300 s, the module SOC is not initialized at the same value, but with a variation of ~ 0.5% around the 15% point. The aim is to highlight the cell balancing with SOC distribution reduction, as shown in Figure 36.

3 HiL VIRTUAL TEST BENCH

3.1 dSPACE HiL TEST BENCH

After validating the SiL approach, plant model and control model must be implemented in a HiL test bench. Tests have been performed with a dSPACE RTI1016 platform.

3.1.1 COMPILATION PROCESS

The HiL model is based on SiL model and 2 additional steps must be performed:

- Generation of files for Real-time platform from Simcenter Amesim
- Compilation with Simulink and RT coder

The first step is mandatory to generate all files needed to correctly link all code in the correct Real-time platform[4]. In this case the platform is a dSPACE ds1006 RT, as shown in Figure 37. All these files are then filled of all datafile link. So, all inputs will be embedded as well as variables to the RT platform.

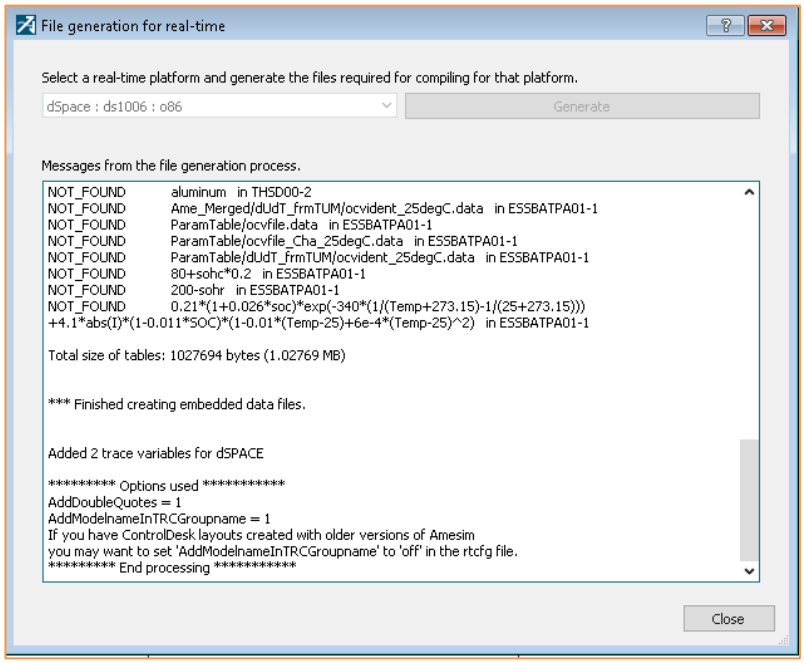

Figure 37: Generation of file for Real-time platform

The second step is the compilation with a Simulink coder. Before compiling the Simulink model with the plant model, a link with the real-time platform must be added on the sketch to ensure data exchange between model and the real-time platform. Then, as shown in Figure 38, specific statements in the code generation tab and in configuration parameters must be updated in order to:

- Specify the system target
- Use the correct makefile template
- write the make command with embedded Simcenter Amesim model

[4] For more information, a dedicated manual us available with Simcenter Amesim [11]

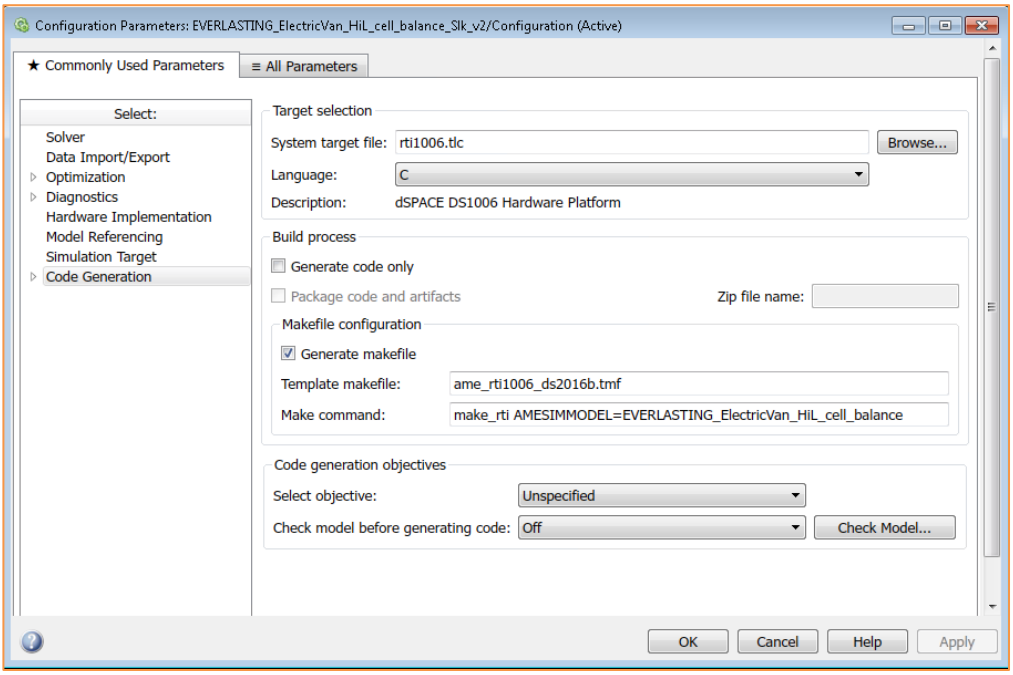

Figure 38: Configuration parameters for code generation

3.1.2 CONTROL DESK INTERFACE

Once code has been generated by the Simulink coder, the HiL virtual test bench can be uploaded to the dSPACE machine to check the validity of the model, meaning model is running in real-time with the correct behaviour. A basic Control Desk layout has been created to highlight the main variables calculated in the model as well as some information of the simulation.

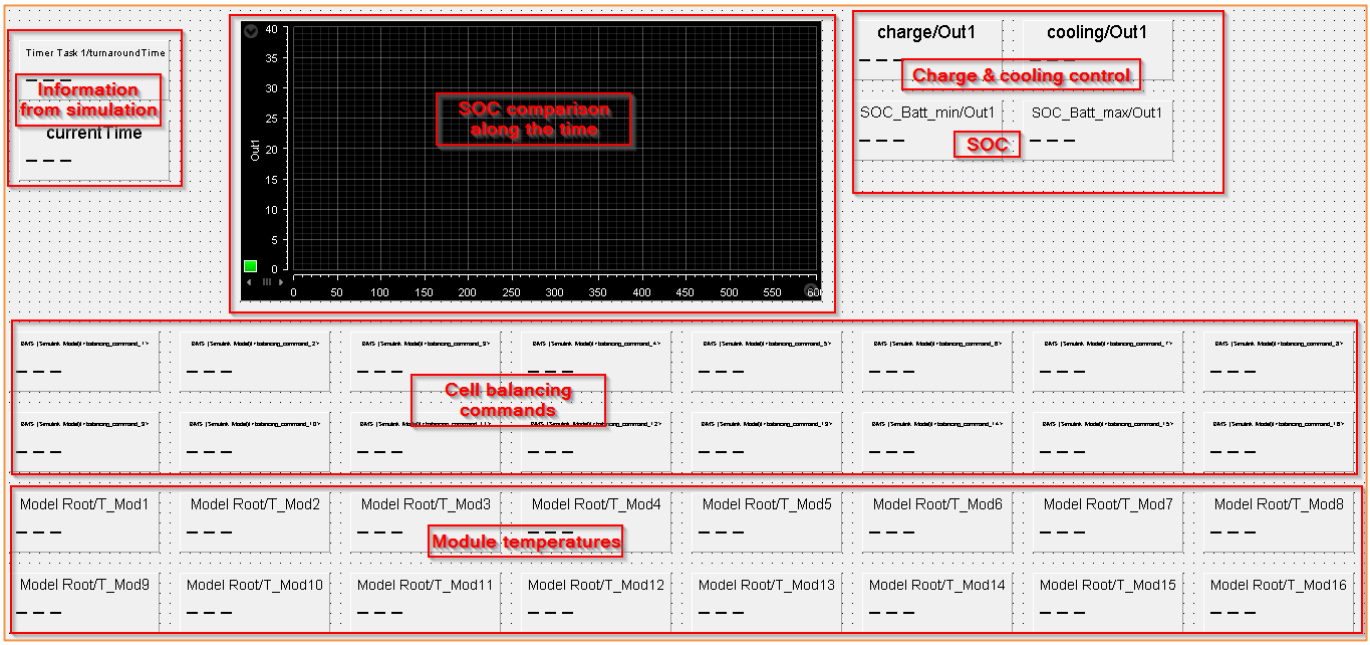

Figure 39: HiL layout with Control Desk

In the current layout shown in Figure 39, several signals are displayed:

- Information from the simulation, like current time or turnaround time
- Charge and cooling function outputs
- Cell balancing command for each module
- Maximal temperature for each module
- Evolution of the minimal and maximal SOC along the time

3.2 HiL Battery Management system test bench

As the HiL model is running in real time, the previous scenario has been split in 2 parts:

- 100 A fast charging scenario with cooling
- WLTC driving cycle

3.2.1 100 A fast Charging scenario with cooling results

Cells balancing are either positive or negative, meaning respectively adding or removing currrent from the battery modules, as shown in Figure 40. In the plot of the SOC, we observe the difference of the SOC, because the tolerance has been set at ~0.1 %.

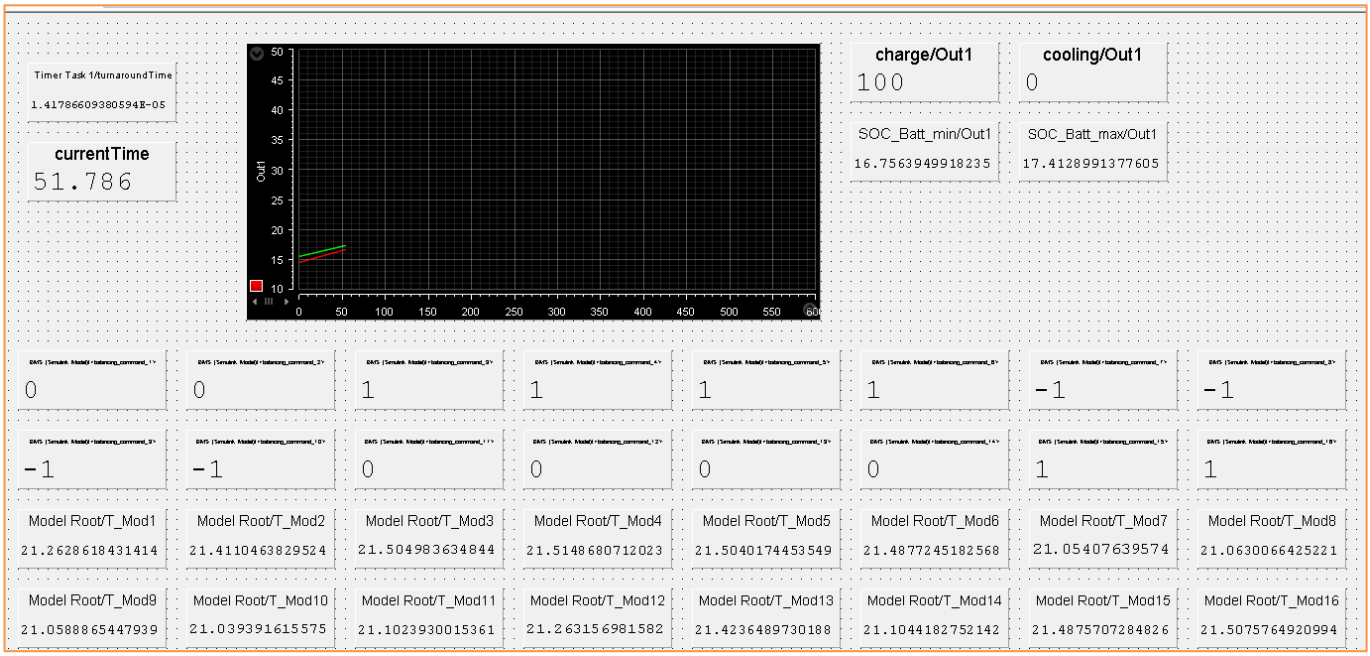

Figure 40: cells balancing highlight results

After 150 s, all modules have been balanced and no more balancing current is supplied to the battery pack. The charge is now homogenous until 730 s, when the maximal module temperature reaches 40 degC. Charging is then stopped to cool down the battery, as shown in Figure 41. We observe that the cooling function was activated as expected and charging current set at 0 A. As a consequence, the SOCs remain constant.

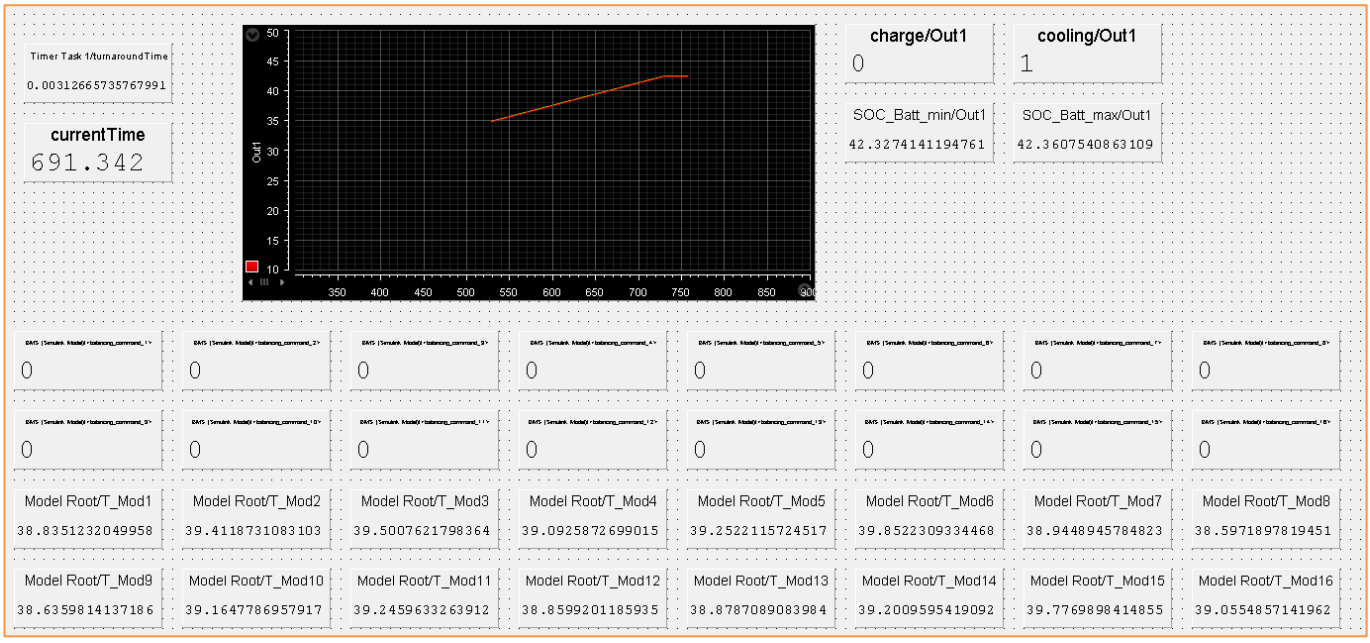

Figure 41: charging & cooling function highlight results

3.2.2 WLTC DRIVING CYCLE RESULTS

HiL virtual test bench has also been validated on a driving cycle to check whether cell balancing is also working when the vehicle is moving. The Control Desk layout has been modified to display vehicle speed compared to driving cycle profile, as shown in Figure 42.

In this scenario, the initial SOC has been set at 55 % with a deviation of 0.5%. We observe the cell balancing during the first 150 s until all SOCs become homogeneous. Furthermore, module temperatures are increasing slower than during the charging scenario. Indeed, the average current is lower during the driving cycle, except at the end, when vehicle is running under Highway conditions.

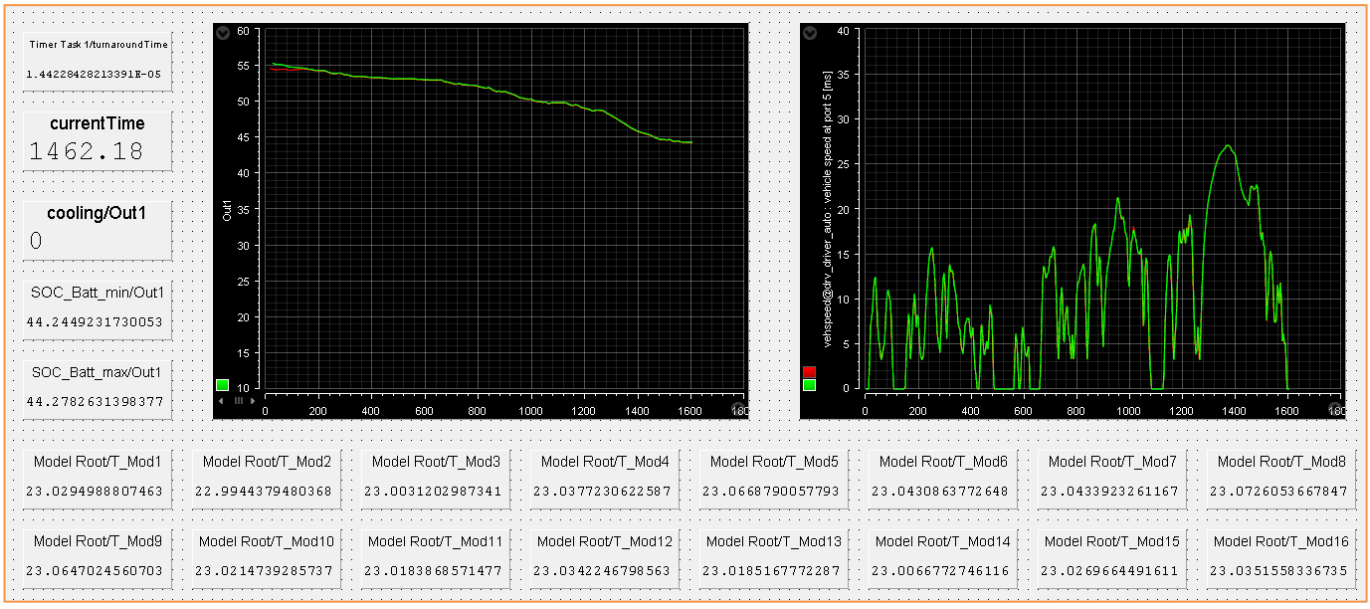

Figure 42: WLTC driving cycle results

CONCLUSIONS

Vehicle models of the Voltia eVan have been developed for different applications, especially for BMS control calibration/validation. Vehicle parameters and electric powertrain measurements have been retrieved from Voltia and TU/e. The battery cell model is originating from TUM and reduced for these virtual test bench models by Siemens.

A focus on detailed battery pack model has been done, to illustrate the control development process through Model in the Loop, Software in the Loop and Hardware in the Loop approaches. Battery module components have been created, using modules in which each contained 3 different sub modules in series. Maximal temperature and module voltage are extracted with virtual sensors and connected to a Simulink interface, where the control is developed both using a SiL and a HiL approach.

Validations of these approaches have been described by following a step-by-step process, especially with regards to real-time scenarios. The described HiL virtual test bench can now relate to BMS hardware for virtual validation, by interfacing with real control.

REFERENCES

[1] JRC, "Electric and hybrid vehicle testing," Joint Research Center, 2018. [Online]. Available: http://publications.jrc.ec.europa.eu/repository/bitstream/JRC109797/jrc109797_final.pdf.

[2] SISW, *Simcenter Amesim Reference guide,* leuven: Siemens Industry Software NV, 2019.

[3] C. Beckers, «D3.3 Report on power request prediction for electric vehicles,» EVERLASTING, Eindhoven, 2020.

[4] J. Sturm, M. C. Donkers et A. Li, «D1.2: Report on model order reduction,» EVERLASTING, Munich, 2019.

[5] J. Sturm, «D1.1 Report on electrochemical cell model,» EVERLASTING, Munich, 2018.

[6] N. S. AP, «A simple Engine Cooling System simulation Model,» *SAE Technical Paper 1999-01-0237,* 1999.

[7] SISW, «Technical bulletin n°102,» Siemens Industry Software NV, Leuven, 2019.

[8] J. Al Koussa, C. De Servi et F. Pra, «D5.3 Report on active cooling modelling & active/passive coupling,» EVERLASTING, Mol, 2018.

[9] A. Alexeev, M. Sachenbacher, L. Riess, D. Behrendt et J. M. Alvarez, «D6.3 Closed source hardware design and prototype,» EVERLASTING, Munich, 2018.

[10] J. Sturm, A. Rheinfield, I. Zilberman, F. B. Spingler, S. Kosh, F. Frie et A. Jossen, «Modeling and Simulation of inhomogeneities in a 18650 nickel-rich, silicon-graphite lithium-ion cell during fast charging,» J. of Power Source, 2019.

[11] SISW, «Real time simulation with Simcenetr Amesim: User's guide,» Siemens Industry Software NV, Leuven, 2019.